CALCULATION OF DOUBLY SCATTERED LIDAR RETURNS

BY

EDWIN WALTER ELORANTA

A thesis submitted in partial fulfillment of the

requirements for the degree of

DOCTOR OF PHILOSOPHY

(Meteorology)

at the

UNIVERSITY OF WISCONSIN

1972

ACKNOWLEDGEMENTS

CALCULATION OF DOUBLY SCATTERED LIDAR RETURNS

Edwin Walter Eloranta

Under the supervision of Professor
James Adolph Weinman

A lidar transfer equation is developed describing the magnitude and polarization of the doubly scattered return signal resulting from the illumination of a homogeneous cloud of spherical particles. Evaluation of the resulting multiple integral for water clouds with model particle size distributions indicates that a significant fraction of the received lidar return is due to double scattering. Both the magnitude and polarization of the calculated return are presented.

The doubly scattered lidar return is shown to be strongly dependent on the ratio of the receiver acceptance angle to the angular width of the forward scattering peak caused by light diffracted around the cloud droplets.

Special case solutions to the double scatter transfer equation are presented. These solutions provide a convenient way to estimate the magnitude of the doubly scattered return for routine lidar work.
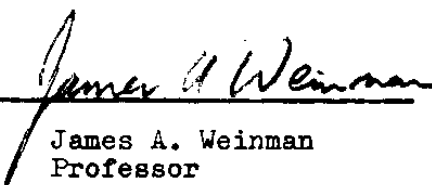
Approved _____

James A. Weinman
Professor

iii

TABLE OF CONTENTS

2. INTRODUCTION

Lidar has been used extensively to probe the atmosphere. Much of the research is summarized in a paper by Collis (1969). The analysis of virtually all lidar data has been based on an equation which assumes that photons returned to the receiver have undergone only a single scattering. The received signal due to multiply scattered photons is assumed negligible.

In general, when measurements of light scattered from small particles are made, van de Hulst (1957) indicates that multiple scattering cannot be safely ignored unless the optical depth of the scattering medium is less than 0.1. Optical depths encountered in atmospheric lidar soundings almost always exceed this limit. Photons returning from a penetration of only 50 meters into a typical cloud are likely to have propagated through an optical depth of nearly ten times this limit. Even on a clear day the optical depth is likely to exceed 0.1 for all returns received from ranges beyond about 400 meters.

Lidar systems usually employ highly collimated transmitters and receivers. Angular beam widths are on the order of 10^{-3} radians. In addition the time duration of the transmitted pulse is short (10^{-8} sec.), and the receivers have small time resolutions (10^{-7} sec.). These lidar features place constraints on the possible propagation paths

of multiply scattered photons, which may reduce the multi-
ply scattered contribution. Because of these constraints,
van de Hulst's optical depth criterion is likely to under-
estimate the actual range of optical depths for which the
single scatter lidar equation is valid. It seems unlikely,
however, that when lidar returns are received from optically
dense media, such as clouds, that propagation constraints
can eliminate multiple scattering. In any case, lidar data
analysis could be placed on a more secure basis by a model
predicting the multiply scattered contribution to a lidar
return. The present paper attempts to fill part of this
need by presenting an easily applied model for the doubly
scattered lidar return from a cloud.

Several authors have calculated multiply scattered
lidar returns. Schotland et al. (1965) computed the doubly
scattered lidar return from the molecular atmosphere.
Curran (1971) treats the doubly scattered lidar return for
both bistatic and monostatic systems. His monostatic cal-
culations assume an aerosol which scatters isotropically
and are limited to cases involving rather small optical
depths. Both Schotland and Curran concluded that the
multiply scattered contribution was negligible for the scat-
tering models they employed. They also suggest that for
other models it might become important. Of most interest
to the present study are the calculations of multiply scat-

tered lidar returns from clouds published by Liou and Schotland (1971) and by Plass and Kattawar (1971).

Liou and Schotland derive an expression for the intensity and polarization of light scattered from a volume element in the laser beam into a second volume in the receiver field of view where it is then scattered toward the receiver. They then obtain the doubly scattered return by summing the contributions from each pair of these incremental volumes which can contribute to the lidar return at a given time. In separate calculations this procedure is extended to the estimation of the third order scattering (Liou, 1971).

Plass and Kattawar (1971) use a Monte Carlo simulation of the exact paths of individual photons to obtain estimates of the lidar return due to all orders of scattering.

Unfortunately the calculations of the above authors provide substantially different estimates for the importance of multiple scattering in lidar returns from clouds. These discrepancies are evident in Fig. 2.1 where their results are illustrated in terms of the multiple to single scatter ratio. Fig. 2.2 presents the particle size distributions used in these determinations. Exact agreement between the curves shown in Fig. 2.1 should not be expected because the authors used different cloud models in their determinations. It appears unlikely, however, that the disagreement shown
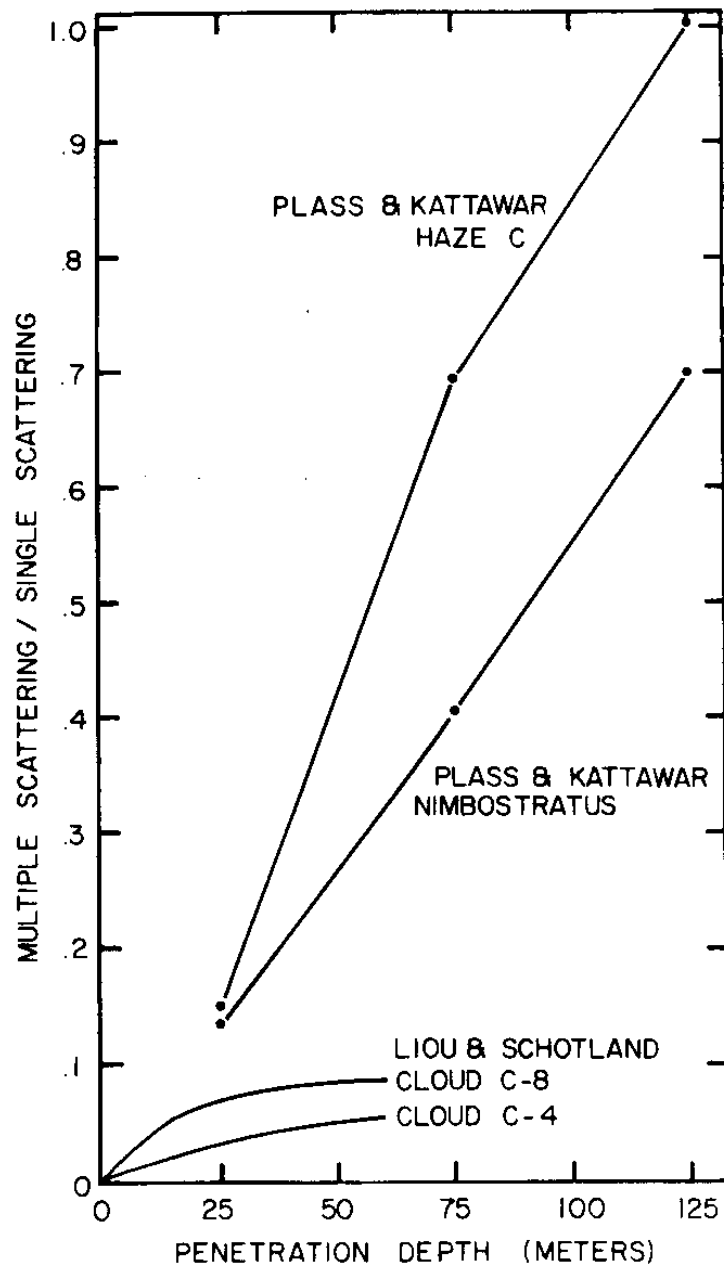
Fig. 2.1 The ratio of multiple to single scattering in a lidar return from a cloud. The extinction cross section per unit volume was 0.01 m^{-1} for the Plass and Kattawar (1971) calculations and 0.0168 m^{-1} for the Liou and Schotland (1971) results.
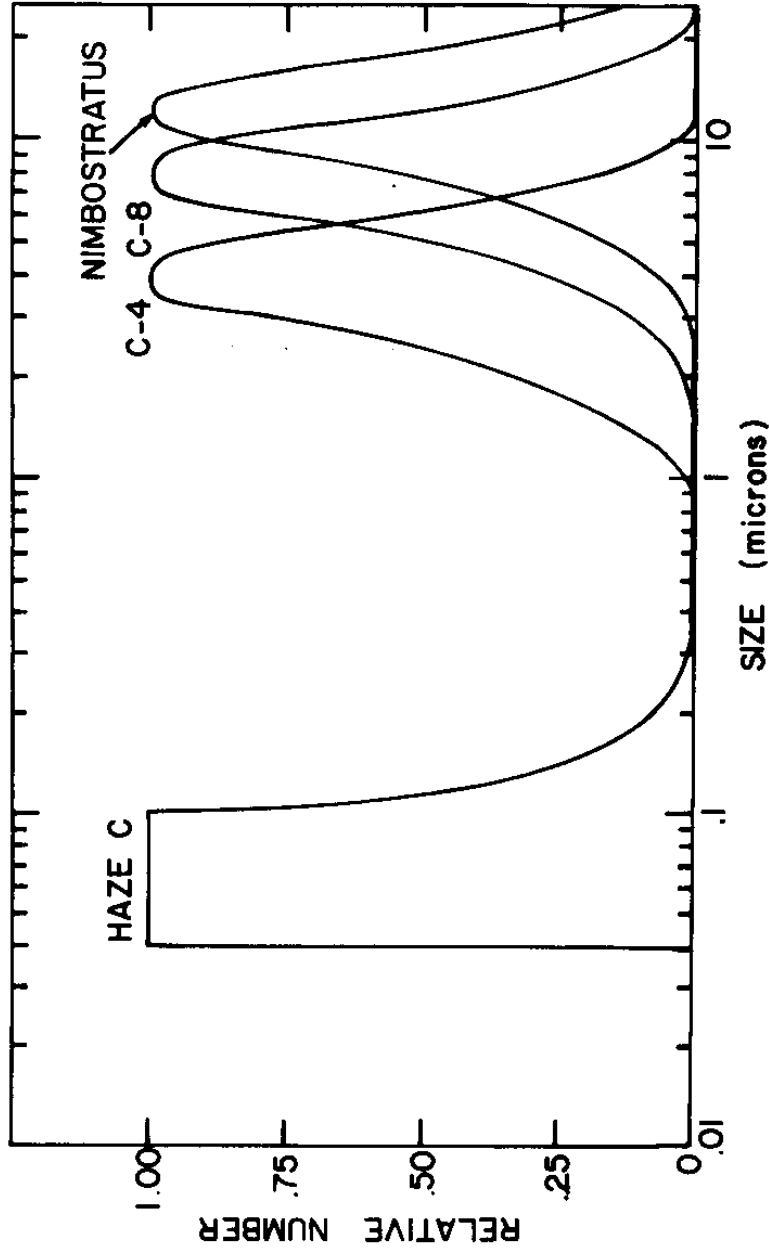
Fig. 2.2 Water droplet size distributions used by Plass and Kattawar (1971) and by Liou and Schotland (1971) to calculate multiply scattered lidar returns.

5

in Fig. 2.1 can be attributed to differences in cloud
models. The particle size distributions used by Liou and
Schotland are intermediate in size to the distributions of
Plass and Kattawar, furthermore, Liou and Schotland assume
a larger scattering cross section in the could than Plass
and Kattawar and should therefore show larger multiple to
single scatter ratios.

The difference between the multiple to single scatter
ratios shown in Fig. 2.1 is of fundamental importance to
the analysis of lidar cloud retunrs. If the calculations
of Liou and Schotland are correct, it appears that, with
the addition of a small correction for multiple scattering,
the single scatter lidar equation is valid for cloud pene-
tration studies. In contrast the Monte Carlo results indi-
cate that the multiply scattered return increases rapidly
as the pulse propagates into the cloud and quickly becomes
comparable in magnitude to the single scattered return.

The remainder of this paper presents the following:
1) a simple intuitive approximation for the ratio of Nth
order scattering to single scattering, 2) a comparison of
this approximation to the results obtained by Lion and
Schotland, 3) a development of a double scatter lidar trans-
fer equation for realistic lidar geometries and homogeneous
clouds of particles which scatter light anisàtropically,
4) simplification of the doubly scattered lidar equation for

easy application in estimating the doubly scattered contribution to a lidar return, 5) typical doubly scattered lidar returns calculated from the transfer function and comparisons with results obtained by other authors.

3.1 Development of a multiple scattering approximation

In this section the multiply scattered contribution to
a lidar return is estimated. This estimate is possible be-
cause approximately one half of the total energy scattered
by cloud droplets is deflected into a narrow diffraction
peak. Small angle approximations are used to calculate the
multiply scattered return due to this portion of the scat-
tered energy.

Consider the geometry of Fig. 3.1 where a laser pulse
illuminates a homegeneous cloud with a base altitude x_c.
Then consider the power incident on the reciever at a time
t after the emission of a laser pulse with a time duration
Δt. Because of a propagation time constraint, singly scat-
tered photons cannot contribute to this signal unless they
have been scattered from a shell of thickness $c\Delta t/2$ located
at a range $ct/2$. As the primary pulse propagates from the
cloud base $(x = x_c)$ to the maximum range $(x = ct/2)$ part of
the pulse energy is scattered by cloud droplets. Thus if
the power transmitted is $\mathcal{P}_0$ and the scattering cross sec-
tion per unit volume of the cloud is β, the power trans-
mitted without scattering to $x = ct/2$ is given by Beer's
law as follows:

3.1 $\mathcal{P} = \mathcal{P}_0 e^{-\beta d}$

where: $d = ct/2 - x_c$.
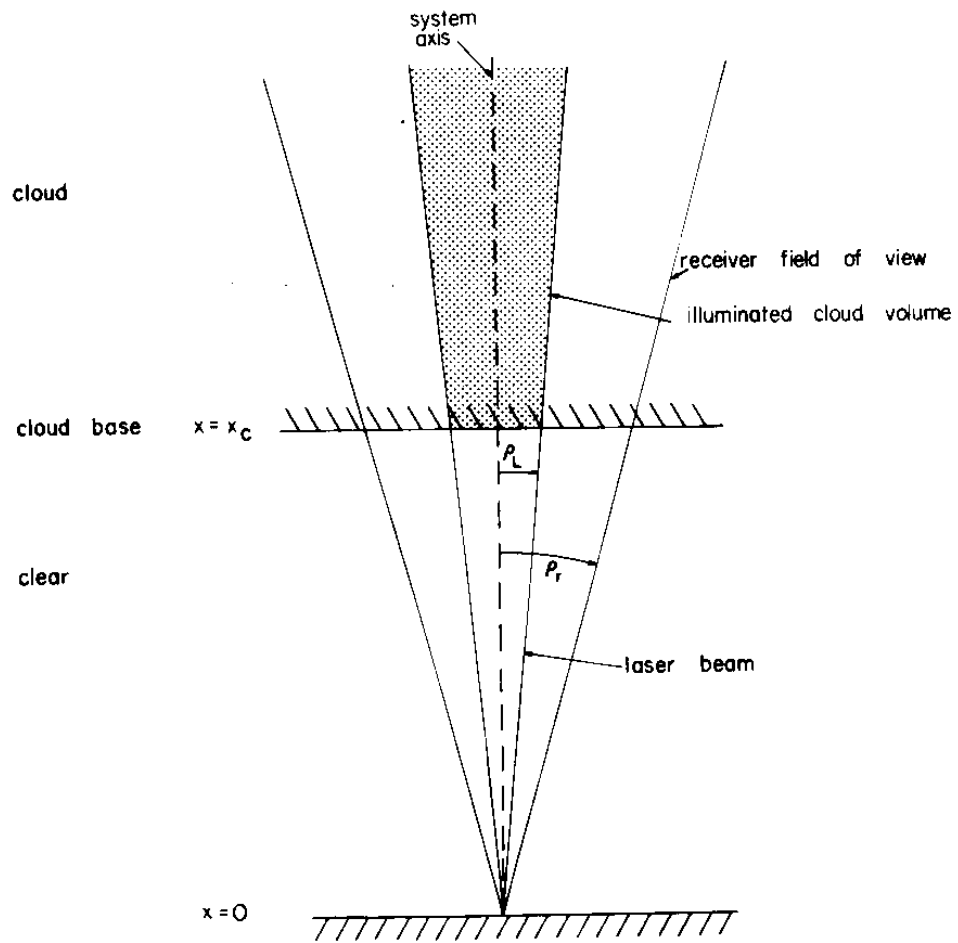
Fig. 3.1 Geometry assumed for estimation of the multiply scattered lidar return.

Not all of the scattered energy is lost from the trans-
mitted beam. Those photons scattered through small angles
continue propagating near the primary beam and travel al-
most the same x-distance as the primary pulse in a given
time interval. Therefore the photons scattered through
small angles arrive at $x = ct/2$ at nearly the
same time as the primary pulse. These scattered photons
differ from the photons of the primary pulse only by having
a wider spatial and angular distribution.

The diffraction peak has an approximate angular half-
width θ_d given by:

$$3.2 \qquad \theta_d = \frac{\lambda}{2r}$$

where: λ = wavelength of the incident radiation

r = radius of the scattering particle.

The water droplet size distributions measured in clouds
usually have a modal radius between 2 and 20 μm; there-
fore, at the ruby laser wavelength ($\lambda = 0.6943 \mu m$) the
angular half-width θ_d of the diffraction peak lies approx-
imately in the range of 0.02 to 0.2 radians. Because θ_d
is small the scattered energy contained in the diffraction
peak is not lost lost from the primary pulse as the pulse
propagates through the cloud layer between x_c and $x = ct/2$.
The apparent optical depth of this layer is therefore only
one half the actual optical depth and Eq. 3.1 can be modi-
fied to give the total power incident at $x = ct/2$ as
follows:

$$3.3 \qquad \beta = \beta_0 \, e^{-\beta d + \beta' d/2}.$$

Fig. 3.2 illustrates the path of a typical multiply scattered photon. The power calculated from equation 3.3 includes contributions due to photons scattered by small angles as well as the directly transmitted photons. For any of them to reach the receiver at a time t after emission of the laser pulse they must undergo a large angle scattering in the slab c∆t/2.

In order to estimate the scattering from this layer, consider a cloud with scattering properties characterized by a Mueller matrix* with elements P_1 and P_2 which satisfy the following:

3.4 $\quad P_1(\theta) \gg P_2(\theta)$ for θ small, and

$\qquad P_1(\theta) \geq P_2(\theta)$ for all other θ

3.5 $\quad P_1(\theta) =$ constant for θ near π radians.

The first condition insures that polarization effects have little influence on the multiple scattering observed with

---

*For a discussion of the scattering matrix and its application to the calculation of electromagnetic scattering from spherical polydispersions see Deirmendjian (1969). The subscript identification of matrix elements used here is defined by Eq. 4.4. The procedure for transforming Deirmendjian's modified matrix elements into the Mueller matrix form used here is presented in Appendix A.
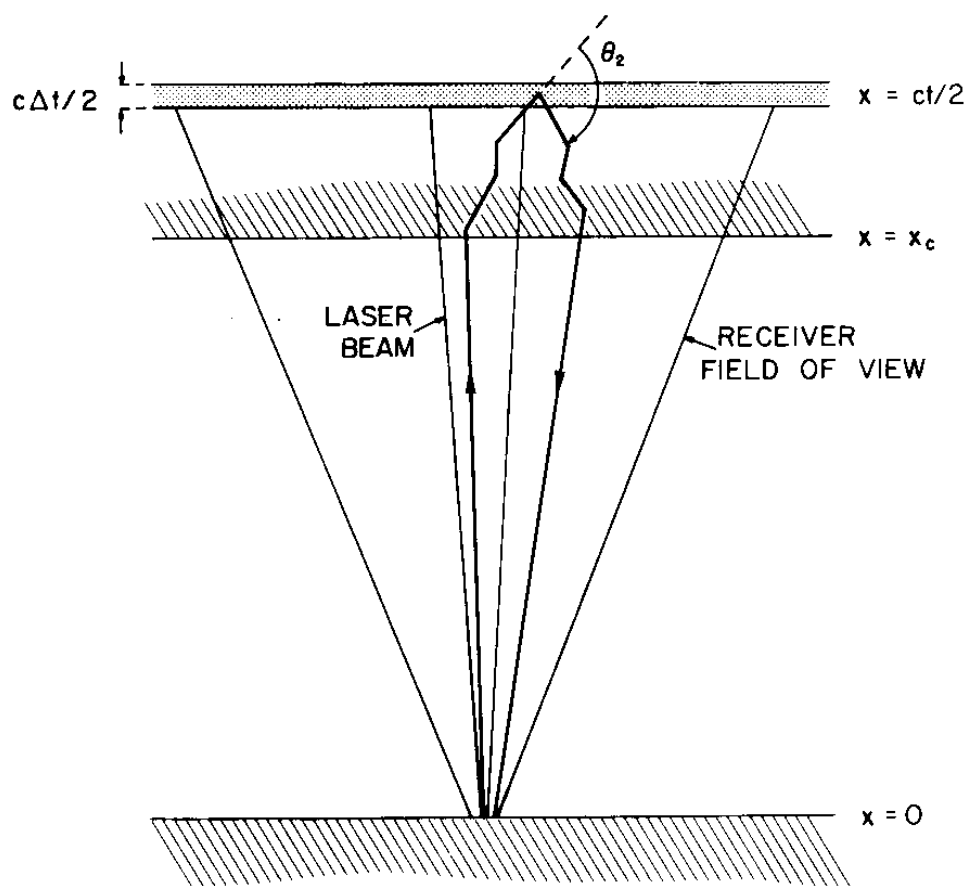
Fig. 3.2 Typical path of a multiply scattered photon.

an unpolarized receiver. An inspection of the matrix
elements presented in Appendix A indicates that condition
3.4 is satisfied for the cloud models considered in this
paper.   The second condition is introduced here only as a
convenience; it considerably simplifies the derivation
which follows, but it is not essential and will later be
discarded. Using condition 3.5, the slab $c \cdot \Delta t/2$ shown in
Fig. 3.2 can be considered a diffusing reflector where a
photon loses all memory of its incident direction.

If the region of this slab illuminated by the transmitted
pulse and the associated small angle scattering is within
the receiver field of view, the power incident on the re-
ceiver without undergoing further scattering is given by:

$$3.6 \quad \beta = \beta_o \cdot e^{-\beta \cdot d + \beta \cdot d/2} \cdot \beta \cdot \frac{c \cdot \Delta t}{2} \cdot \frac{P_1(\pi)}{4\pi} \cdot \omega_r \cdot e^{-\beta \cdot d}$$

where: β = the scattering cross section per unit volume

$P_1(\pi)$ = the value of the scattering phase function
   at π radians

ω_r = solid angle subtended by receiver when viewed
   from the slab $c \cdot \Delta t/2$.

The additional $e^{-\beta d}$ term accounts for the fraction of the
photons scattered while propagating out of the cloud; how-
ever, some of these scattered photons also fall on the re-
ceiver aperture and are not lost. Most of the photons
which are scattered in traversing out of the cloud but
which nevertheless contribute to the received signal leave

the slab at angles near the system axis. They are then
scattered through small angles into the receiver. A photon
which leaves the slab at an angle near the system axis and
then undergoes a large angle scattering is likely to pro-
pagate out of the receiver field of view before undergoing
another large angle scattering which directs it back towards
the reciever. In the same manner, a photon which leaves the
slab at a large angle to the receiver axis is likely to pro-
pagate out of the field of view before undergoing a scat-
tering which could direct it towards the receiver. If the
cloud altitude x_c is much larger than the penetration depth
d, such that the solid angle ω_r subtended by the receiver
varies little with position in the layer between x_c and
ct/2, small angle scattering serves only to redistribute
the already almost isotropic light scattered from the slab.
The photons scattered away from the receiver by small angle
scattering are compensated for by the other photons scat-
tered into the receiver by small angle scatterings. Small
angle scattering therefore, does not contribute to the
attenuation of the pulse as it propagates out of the cloud,
and the total power falling on the receiver can be written
as:

$$3.7 \quad \beta = \beta_o e^{-\beta \cdot d + \beta \cdot d/2} \cdot \beta \cdot \frac{c \cdot \Delta t}{2} \cdot \frac{P_i(\pi)}{4\pi} \cdot \omega_r \cdot e^{-\beta \cdot d + \beta \cdot d/2} .$$

After combining the $e^{-\beta d}$ terms and expanding in a power

3.8 $\quad \mathcal{G} = \mathcal{G}_0 \cdot \dfrac{c \cdot \Delta t}{2} \cdot \omega_r \cdot \beta \cdot \dfrac{P_1(\pi)}{4\pi} \cdot e^{-2\beta d} \left(1 + \beta \cdot d + \dfrac{(\beta \cdot d)^2}{2!} + \ldots \right).$

If the following identifications are then made:

$\omega_r = A/r^2$ = solid angle subtended by receiver

$\beta \cdot \dfrac{P_1(\pi)}{4\pi} = \beta'_\pi$ = backscatter cross section

$\beta \cdot d = \int_0^r \beta \, dr'$ = optical thickness

where: A = area of the receiver

$r = ct/2,$

then the first term of Eq. 3.8 is the usual lidar equation for the singly scattered lidar return as presented by Collis, (1969). The other terms in this equation represent contributions due to multiple small angle scattering. Since the probability of N scatterings occuring in a layer with optical depth $\beta \cdot d$ is proportional to $(\beta \cdot d)^N$, the succesive terms of the power series can be identified as the contributions due to successively higher orders of scattering. Thus the ratio of the N$^{\text{th}}$ order contribution, $\mathcal{G}_N$, to the singly scattered return, $\mathcal{G}_1$, can be written:

3.9 $\quad \mathcal{G}_N / \mathcal{G}_1 = \dfrac{(\beta \cdot d)^{N-1}}{(N-1)!}.$

Condition 3.4 was applied in the development of this equation, therefore the matrix element $P_1(\theta)$ has been set equal to its value at π radians for all angles near π radians. Inspection of the matrix elements presented in Appendix A shows that this is a relatively crude approx-

imation. A correction can now be applied to these ratios
to eliminate the need to assume isotropic scattering near π.
The scattering phase function describing the large angle
scattering in this slab should be the average value of $F_1(\theta)$
encountered by photons returned to the receiver after N scat-
terings rather than the value at π. With this correction
the ration presented in Eq. 3.9 becomes:*

3.10
$$\frac{G_N}{G_1} = \frac{\langle P_1(\pi)\rangle_N}{P_1(\pi)} \cdot \frac{(\beta \cdot d)^{N-1}}{(N-1)!}$$

where $\langle P_1(\pi)\rangle_N$ is the weighted mean of the matrix element P_1
near the backscatter direction, given by

3.11
$$\langle P_1(\pi)\rangle_N = 2\pi \int_0^\pi M_N(\theta_1) \, P_1(\pi - \theta_1) \cdot \sin(\theta_1) \, d\theta_1$$

and $M_N(\theta_1)$ is the probability that a photon scattered N
times undergoes a scattering at an angle θ_1 in the slab
$c\Delta t/2$. The (N-1) small angle scattering events which each
produce an angular deflection less than θ_d can produce a
maximum angular deviation $(N-1)\theta_d$. Therefore, in order to
allow a photon to return to the receiver, the large angle

---

*This equation could have been derived directly without
using the isotropic backscattering assumption expressed by
condition 3.5. However, in that case it would be necessary
to consider each order of scattering separately and further-
more to break each scattering order into all of the possible
combinations of scattering events with n scatterings before
and m scatterings after the large angle event, where
n+m = N-1. In either case the same expression results.

CORRECTION

≡ RATIOS

scattering, which takes place in the slab $c\Delta t/2$ must produce a deflection greater than $\pi - (N-1)\theta_d$. The distribution function $M_N(\theta)$ must therefore satisfy the condition

3.12 $\quad M_N = 0 \quad$ for $\quad \theta < (N-1) \cdot \theta_d$.

For the special case $N = 2$, $M_N(\theta)$ can be calculated exactly. Only two possible scattering conditions exist: a single small angle scattering followed by a large angle scattering in the slab $c \cdot \Delta t/2$, or else a large angle event in the slab followed by a small angle scattering. In either case the probability distribution $M_2(\theta)$ is determined by the scattering phase function near 0 rad and can be calculated as follows:

3.13 $\quad M_2(\theta_i) = \dfrac{P_1(\theta)}{2\pi \displaystyle\int_0^{\theta_d} P_1(\theta_i) \cdot \sin(\theta_i) \cdot d\theta_i}, \quad \theta_i \le \theta_d$

$M_2(\theta_i) = 0, \quad \theta_i > \theta_d$.

After a large number of scatterings Rossi (1952) shows that the angular distribution of photons becomes Gaussian. The probability distribution $M_N(\theta)$ is then given by

3.14 $\quad M_N(\theta_i) = \left(\dfrac{1}{K}\right) \cdot e^{-\theta_i^2 / \langle \theta^2 \rangle_N}$

where

3.14a $\quad K = 2\pi \int_0^{\theta_d \cdot (N-1)} e^{-\theta_i^2/\langle\theta^2\rangle_N} \cdot \sin(\theta) \cdot d\theta$

and

3.15 $\quad \langle\theta_1^2\rangle_N = (N-1) \cdot \int_0^{\theta_d} \theta^2 \cdot P_1(\theta) \cdot \sin(\theta) \cdot d\theta \bigg/ \int_0^{\theta_d} P_1(\theta) \cdot \sin\theta \cdot d\theta.$

Because the initial shape of the diffraction peak is nearly Gaussian*, this relation can be expected to hold true even for small values of N.

Eq. 3.10 can now be used to estimate the relative contribution due to individual orders of multiple scattering. Two major assumptions are implicit in these estimates:

1) The dominant contribution to the multiply scattered return consists of photons which undergo only a single large angle scattering.

2) The angular field of view of the receiving telescope satisfies the following condition

3.16 $\quad \rho_r \geq \dfrac{(N-1) \cdot \theta_d \cdot d}{x_c} + \rho_L$

where $2\rho_L$ = the transmitted beam divergence.

This condition expresses the requirement that after N-1 scatterings, each with angle less than θ_d the scattered photon is still within the receiver field of view. For most lidar configurations this requirement restricts application of Eq. 3.10 to relatively small penetration depths.

---

*In appendix A, for several particle size distributions, comparisons are made between exact values of $P_1(\theta_1)$ and a Gaussian fit to these functions.

3.2 A comparison with other multiple scattering
    calculations

In Fig. 3.3 the approximate multiple scattering equation (3.10) is compared to the double scatter calculations published by Liou and Schotland (1971). Both calculations assume a homogeneous water cloud with a particle size distribution given by the cloud model C-1 (Appendix A). The scattering cross section per unit volume β_s is equal to 0.0168 m^{-1}. The scattering matrix elements presented in Appendix A and Eq. 3.11 were used to obtain the matrix elements required by the approximation. The backscatter value of P_1 and the average values used are

3.17
$$\frac{P_1(\pi)}{4\pi} = 0.05 \qquad \frac{\langle P_1(\pi)\rangle_2}{4\pi} = 0.035$$

$$\frac{\langle P_1(\pi)\rangle_3}{4\pi} = 0.035 \qquad \frac{\langle P_1(\pi)\rangle_4}{4\pi} = 0.034$$

The maximum angular deflection within the diffraction peak was estimated as 4° by visual inspection of the scattering matrix elements. This value is needed to determine the mean square scattering angle with Eq. 3.15.

The lidar system assumed in calculations by Liou and Schotland transmitted a pulse with a Gaussian angular distribution. Only 80% of the transmitted energy was assumed to fall within the receiver field of view. Because the
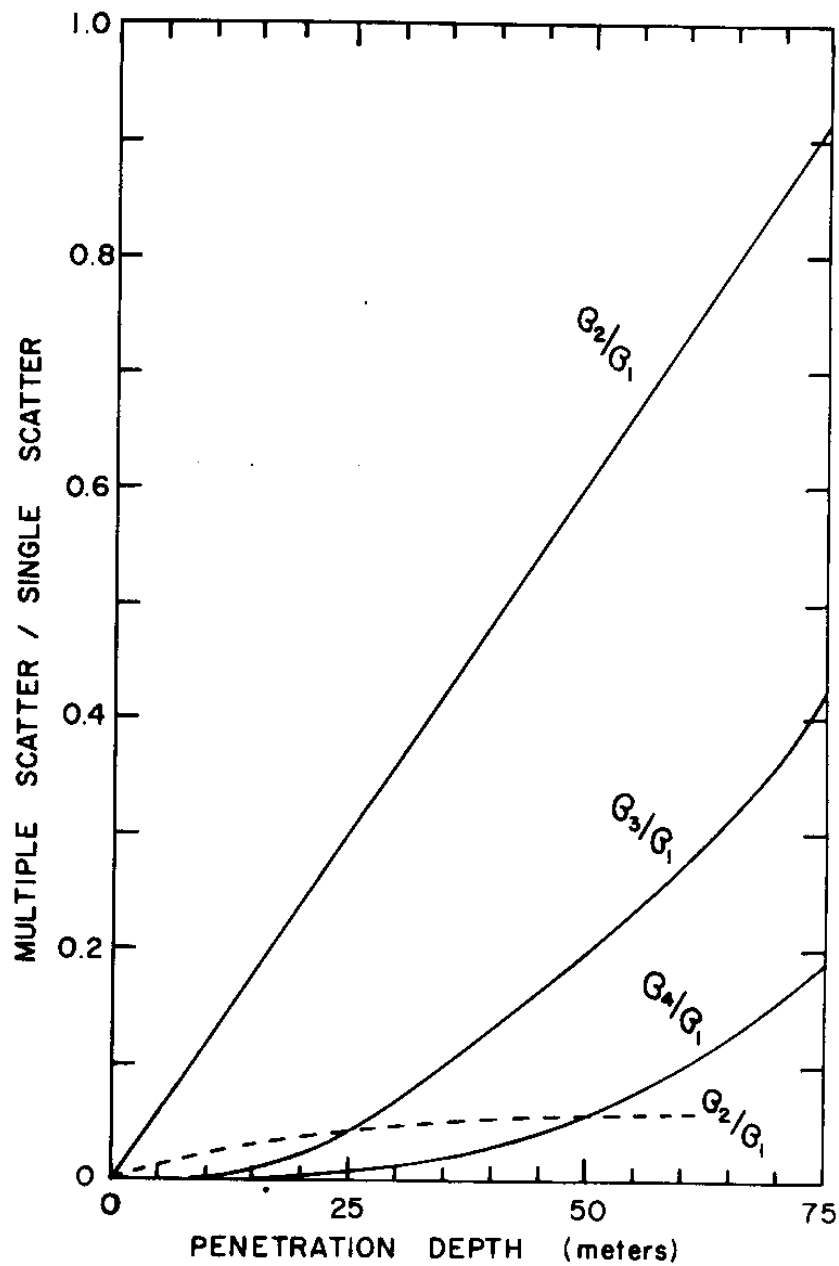
Fig. 3.3 A comparison of the multiple to single scatter ratios, G_M/G_1, predicted by Eq. 3.10 (solid lines) and the ratios calculated by Liou and Schotland (dashed line). The values of G_3/G_1 derived by Liou and Schotland are approximately one tenth as large as their G_2/G_1 values.

assumed laser beam divergence was larger than the receiver field of view, condition 3.16 shows that the approximate solution (Eq. 3.10) is not directly applicable. However, failure to satisfy this condition can not explain the **more** than ten-fold disagreement between the double scatter estimates shown in Fig. 3.2. Consider the doubly scattered contribution from that portion of the transmitted pulse inside a 5 milliradian cone. If θ_d is conservatively estimated as 4°, condition 3.16 is satisfied up to a penetration depth of 36 m for the inside half of the transmitted beam. The double scatter contribution from this portion of the beam can be estimated with Eq. 3.10. Since 30% of the transmitted energy* is contained in this 5 milliradian cone, **the** ratio θ_2/θ_1 can be estimated for the inner portion of the transmitted beam by multiplying the values in Fig. 3.2 by 0.30. Clearly, this estimate, which considers only a **small** portion of the transmitted pulse, **also yields a ratio of double to single scattering much larger than that obtained by Liou and Schotland. Thus the discrepancy which appears in Fig. 3.2 cannot be attributed to the failure of this system to satisfy condition 3.16.**

An attempt was also made to compare the approximate

---

*A Gaussian beam with 80% of its energy contained in a 10 milliradian cone, has 30% of the energy inside a 5 milliradian cone.

results obtained from Eq. 3.10 to the Monte Carlo determina-
tion of multiple scattering published by Plass and Kattawar
(1971). Comparisons were possible only for the homogeneous
cloud model composed of droplets with a nimbostratus model
size distribution (Fig. 2.2). The values of $\langle P_1(\pi) \rangle_N$ required
by Eq. 3.10 were difficult to obtain from the graph of
scattering matrix elements presented by **Kattawar** and **Plass**
(1968). These values were obtained by visual estimates
and contained uncertainties as large as a factor of two.
Within the limits of this uncertainty Eq. 3.10 provides a
multiply scattered return which agrees with the Monte Carlo
estimates presented in Fig. **2.1.**

4. DERIVATION OF A GENERAL TRANSFER FUNCTION FOR DOUBLE SCATTERING

The double scattered contribution to a lidar return from a homogeneous cloud of spherical particles will now be calculated in exact form. These calculations assume the coaxial system geometry shown in Fig. 3.1. Details of the scattering geometry are illustrated in Figs. 4.1 and 4.2. The radiant power doubly scattered, first from the primary beam in the incremental volume dV_1 into the volume element dV_2 and then from dV_2 into the receiver, is calculated. The resulting expression is integrated over the volume included in the transmitted beam and the reciever field of view to obtain the doubly scattered power incident on the receiver.

Incoherent scattering is assumed; therefore the magnitude and polarization of the doubly scattered return can be represented by means of a Stokes vector[*], I_o. The derivations in this paper will use the Stokes vector with components I, Q, U, V as defined by Shurcliff (1962) rather than the modified I_1, I_r, U, V form used by Chandrasekhar (1960) and Deirmendjian (1969). This form of the vecotr was chosen because it simplified the development which follows.

4.1 A Stokes vector description of the transmitted laser pulse

---

[*]See Appendix B
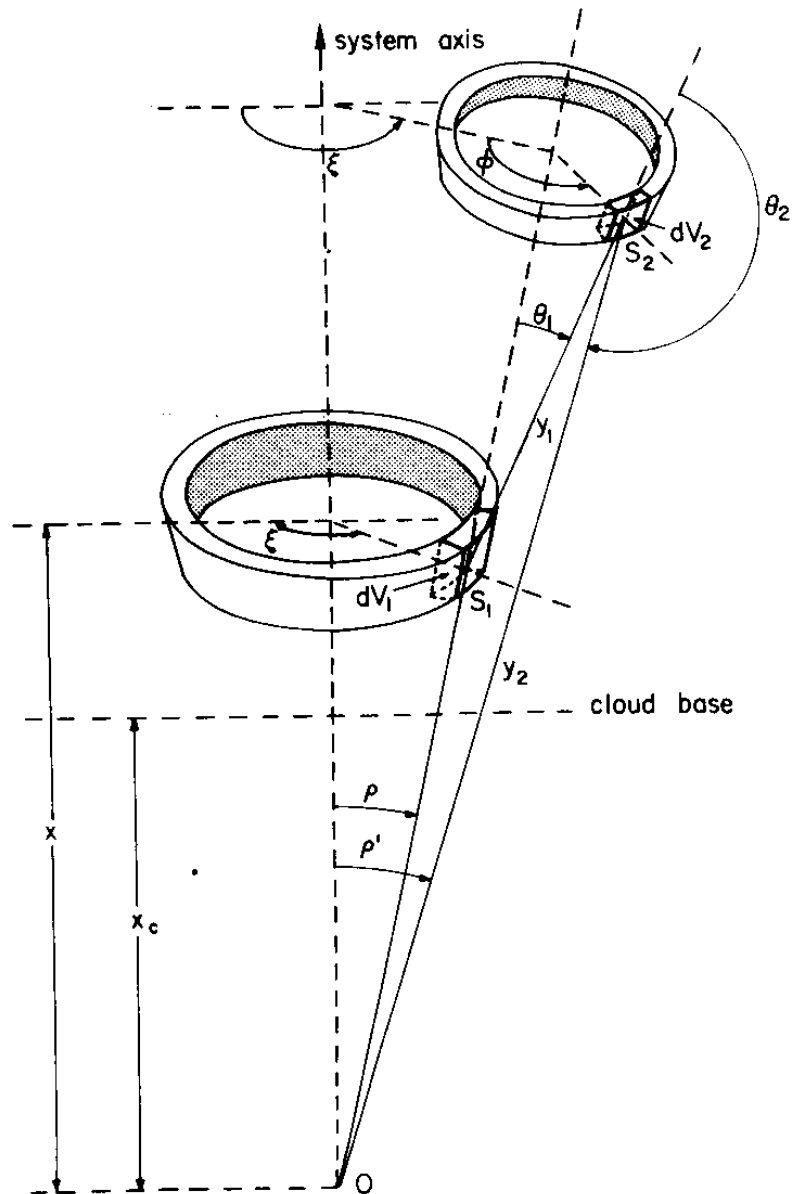
Fig. 4.1 Geometry used for double scatter integration. The lidar is located at point O. The incremental scattering volumes are specified by spherical coordinates, x secρ,ρ, ξ, for the first volume DV_1 and y,θ,ϕ for the second volume, dV_2.
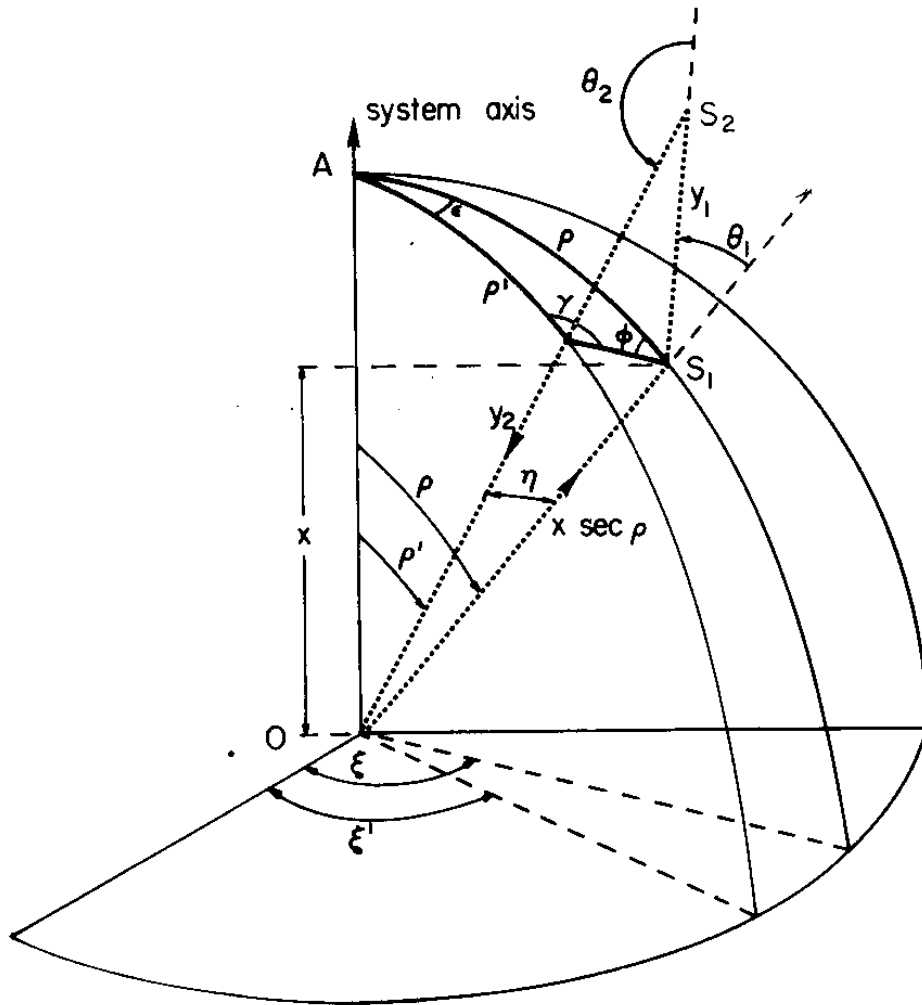
Fig. 4.2 Double scatter geometry defining Stokes vector reference planes and rotations required for transformations between these planes. Lidar is located at point O with the first scattering at S_1 and the second scattering at S_2. Transmitted Stokes vector is referenced to plane O,A,S_1, the receiver response to plane O,A,S_2, and the scattering plane is O,S_1,S_2.

As the first step in the double scatter derivation the
magnitude and the polarization of the transmitted laser
energy must be represented in a vector form for all trans-
mitted propagation directions (ρ,ξ). The transmitted Stokes
vectors will be defined in terms of the reference directions
used by Chandrasekhar (1960). These reference directions
are defined by a pair of axes, both perpendicular to the
plane containing the propagation direction and the system
axis (plane O,A,S_1 in Fig. 4.2). The polarization and rel-
ative angular distribution of the transmitted intensity are
assumed time independent. The transmitted polarization is
also assumed independent of the angular displacement from
the system axis. With these assumptions, if the distribution
of transmitted energy is radially symmetric and the beam is
linearly polarized, the transmitted Stokes vector $\vec{I}_0$ can be
written:*

4.1 $\qquad \vec{I}_0 = \beta_0(t - R/c) \cdot q(\rho) \cdot \begin{pmatrix} 1 \\ \cos 2\xi \\ \sin 2\xi \\ 0 \end{pmatrix}$

where ρ, ξ and x are defined in Fig. 4.1, and

$\qquad$ c = speed of light

$\qquad \beta_0(t)$ = transmitted power (watts)

$\qquad$ R = propagation distance from laser

---

*To an observer looking into the laser from an angular
position in the beam ρ,ξ, the transmitted light described
by Eq. 4.1 will appear linearly polarized with the electric
field vector normal to the propagation direction and rotated
counter clockwise by an angle $\pi/2 - \xi$ with respect to the
O,A,S plane (Fig. 4.2).

t = time

g(ρ) = relative angular distribution of trans-

mitted intensity (1/str.).

The angular distribution function g(ρ) is normalized such that

$$4.2 \qquad \int_0^{2\pi} d\xi \int_0^{\rho_r} g(\rho) \cdot \sin\rho \cdot d\rho = 1$$

4.2 The basic double scatter integral

The Stokes vector $\vec{dI}$ describing the intensity scattered from dV_1 to dV_2 and then from dV_2 to the receiver is found using the linear transformations of Chandrasekhar (1960), adapted to the I,Q,U,V form of the Stokes vector*.

$$4.3 \qquad \vec{dI} = \beta_s^2 \cdot \left(\frac{1}{y_1^2 \cdot x^2 \cdot \sec^2\rho}\right) \cdot e^{-\beta_E(R - x \cdot (\sec\rho + \sec\rho'))}$$

$$\frac{\widetilde{P(\theta_2)}}{4\pi} \cdot \frac{\widetilde{P(\theta_1)}}{4\pi} \cdot \widetilde{L(-\phi)} \cdot \vec{I_o} \cdot dV_1 \cdot dV_2$$

where y_1, y_2, ρ', θ_2, θ_1, and ϕ are defined in Fig. 4.1

and β_s = scattering cross section per unit volume

β_E = extinction cross section per unit volume

$\widetilde{P}(\theta)$ = scattering matrix (Deirmendjian, 1964) adapted

to I,Q,U,V form of Stokes vector. (Appendix A)

---

*The transformation which converts matrices defined in the I_l, I_r, U, V form into the I,Q,U,V form is discussed in Appendix A.

4.4
$$\mathbb{P}(\theta) = \begin{pmatrix} P_1 & P_2 & 0 & 0 \\ P_2 & P_1 & 0 & 0 \\ 0 & 0 & P_3 & P_4 \\ 0 & 0 & -P_4 & P_3 \end{pmatrix}$$

$$R = x \sec \rho + y_1 + y_2$$

$L(-\phi)$ = the matrix which transforms the Stokes

vector into a coordinate system rotated

in a right hand direction by an angle

$(+\phi)$ about the propagation direction

(Shurcliff, 1962).

4.5
$$L(-\phi) = \begin{pmatrix} 1 & 0 & 0 & 0 \\ 0 & \cos 2 & -\sin 2 & 0 \\ 0 & \sin 2 & \cos 2 & 0 \\ 0 & 0 & 0 & 1 \end{pmatrix}$$

4.6
$$y_2^2 = x^2 \cdot \sec^2 \rho + y_1^2 + 2 \cdot y_1 \cdot x \cdot \sec \rho \cdot \cos \theta_1$$

The vector intensity $\vec{dI}$ calculated from Eq. 4.4 is
referenced to an axis perpendicular to the direction ρ', ξ'
and perpendicular to the scattering plane $(0, S_2, S_1)$.
Because the scattering plane orientation changes with

changes in the position of dV_1 and dV_2, $\vec{dI}$ must be trans-

formed to a set of fixed coordinates before an integration

over scattering volumes can be performed. It is convenient

to rotate $\vec{dI}$ by an angle $\pi - \delta$ (Fig. 4.2) to a new pair

of axes also perpendicular to the direction ρ', ξ' but now

with one axis contained in the plane O,A,S and the other

axis perpendicular to this plane. The receiver response

to intensity incident from the direction ρ', ξ' and referenced

to this set of axes can then be described with the operator

4.7 $\quad \hat{u} \cdot \widetilde{T(\rho', \xi')}$

Where $\widetilde{T(\rho, \xi)}$ is the Mueller matrix* describing the receiver characteristics and $\hat{u} = (1,0,0,0)$. The unit vector $\hat{u}$ arises in this expression because photodetectors respond to only the first component of the Stokes vector. Operating on Eq. 4.3 with Eq. 4.7 and multiplying by the solid angle subtended by the receiver aperture when viewed from S_2 yields an expression for the power incident on the receiver, $d\mathcal{P}_2$, due to scattering from dV_1 and dV_2 and then from dV_2 to the receiver. For S_2 in the receiver field of view:

4.8 $\quad d\mathcal{P}_2 = \beta_s^2 \cdot \tan\rho \cdot \sin\theta \cdot \dfrac{A}{y_2^2} \cdot e^{-\beta_E \left(R - x_c(\sec\rho + \sec\rho')\right)}$

$$\cdot \hat{u} \cdot \widetilde{T(\rho, \xi)} \cdot \widetilde{L(\delta - \pi)} \cdot \widetilde{P(\theta_2)} \cdot \widetilde{L(-\phi)} \vec{I}_o \, d\rho \cdot d\xi \cdot dx \cdot d\phi \cdot dy_j$$

For S_2 outside the receiver field of view

4.9 $\quad d\mathcal{P}_2 = 0$

Where A = area of receiver aperture and the geometry of Fig. 4.1 has been used to derive the following:

---

*A procedure for calculating the Mueller matrix for a complex optical system is described by Priebe (1970).

$$4.10 \quad dV_1 = x^2 \cdot \sec^3\rho \cdot \sin\rho \cdot d\rho \cdot d\xi \cdot dx$$

$$4.11 \quad dV_2 = y_1^2 \cdot \sin\theta_1 \cdot d\theta_1 \cdot d\phi \cdot dy_1$$

Consider an ideal receiver characterized by the following Mueller matrix:

$$4.12 \quad \widetilde{T}(\rho', \xi') = \widetilde{F} \cdot \widetilde{L}(\xi')$$

Where $\widetilde{F}$ is the Mueller matrix describing a filter used by the receiver to analyze the polarization of the incoming signal (Shurcliff, 1962). The geometry of Fig. 4.2 indicates that a rotation ξ' about O,A is equivalent to a rotation $-\xi$ followed by a rotation ϵ; therefore

$$4.13 \quad \widetilde{L}(\xi') = \widetilde{L}(-\xi) \cdot \widetilde{L}(\epsilon) = \widetilde{L}(\epsilon - \xi)$$

Using Eqs. 4.12 and 4.13 the matrix operation of Eq. 4.8 can be written:

$$4.14 \quad \hat{u} \cdot \widetilde{T}(\rho', \xi) \cdot \widetilde{L}(\gamma - \pi) \cdot \frac{\widetilde{P}(\theta_2)}{4\pi} \frac{\widetilde{P}(\theta_1)}{4\pi} \cdot \widetilde{L}(-\phi) \cdot \vec{I}_0$$

$$= \mathcal{G}_0(t - R/c) \cdot g(\rho) \cdot \hat{u} \cdot \widetilde{F} \cdot \frac{\vec{S}(\psi, \chi, \theta_1, \theta_2)}{16\pi^2}$$

where $-\psi = \phi' + \xi$

For economy of notation the definition

$$4.15 \quad \phi' = \pi - \gamma - \epsilon$$

is introduced. The vector $\vec{S}$ is given by

4.16

$$\vec{S}(\psi, \chi, \theta_1, \theta_2) = \begin{bmatrix} P_1(\theta_2)\{P_1(\theta_1) + P_3(\theta_1)\cos 2\chi\} + P_2(\theta_2)\{P_2(\theta_1) + P_4(\theta_1)\cos 2\chi\} \\[4pt] \cos 2\psi\left[P_2(\theta_2)\cdot\{P_1(\theta_1) + P_3(\theta_1)\cos 2\chi\} + P_1(\theta_2)\{P_2(\theta_1) + P_4(\theta_1)\cos 2\chi\}\right] - \sin 2\psi\left[P_3(\theta_2)P_3(\theta_1)\sin 2\chi - P_4(\theta_2)P_4(\theta_1)\sin 2\chi\right] \\[4pt] \sin 2\psi\left[P_2(\theta_2)\cdot\{P_1(\theta_1) + P_3(\theta_1)\cos 2\chi\} + P_1(\theta_2)\{P_2(\theta_1) + P_4(\theta_1)\cos 2\chi\}\right] + \cos 2\psi\left[P_3(\theta_2)P_3(\theta_1)\sin 2\chi - P_4(\theta_2)P_4(\theta_1)\sin 2\chi\right] \\[4pt] -P_4(\theta_2)P_3(\theta_1)\sin 2\chi - P_3(\theta_2)P_4(\theta_1)\sin 2\chi \end{bmatrix}$$

where $\quad -\chi = \phi + \xi$.

Substituting Eq. 4.14 into Eq. 4.8 and integrating the spatial coordinates $\rho, \theta_1, \phi, \chi, y$ and ξ over the volume common to the cloud and the receiver field of view leads to the following equation for doubly scattered power incident on the photodetector of the receiver:

$$\mathcal{P}_2(t) = A\,\hat{\beta}_s^2\cdot\hat{u}\cdot\tilde{F}\cdot\int_0^{\rho r} g(\rho)\cdot\tan\rho\cdot d\rho\int_0^{\pi}\sin\theta_1\cdot d\theta_1\int_0^{2\pi}d\phi$$

4.17
$$\cdot\int_0^{\infty}dx\int_0^{y_{1max}}\frac{\mathcal{P}_0(t-R/c)}{y_2^2}\cdot e^{-\beta_E(R-x_c(\sec\rho+\sec\rho'))}dy_1$$

$$\cdot\int_0^{2\pi}\frac{\vec{S}}{16\pi^2}\cdot d\xi$$

where $y_{1\,max}$ is the distance a photon scattered at point S_1 in a direction θ_1, ϕ can travel without leaving either the receiver field of view or the cloud. Eq. 4.17 is the basic double scatter integral. The remainder of section 4 will be devoted to reducing this cumbersome multiple integral to a more usable form.

4.3 An upper limit of integration for the y_1-integral

The upper integration limit for the y_1-integral, $y_{1\,max}$,

is the distance a photon can travel from S_1, in a direction θ_1, ϕ , before it leaves the cloud volume visible to the receiver. This limit is determined in one of three ways depending on whether the photon 1) propagates out of the receiver field of view before leaving the cloud, 2) travels up into the cloud nearly parallel to the system axis such that it never leaves the field of view, or 3) escapes through the cloud base before leaving the field of view.

In the first case where the limit is determined by the edge of the receiver field of view the following equation involving $y_{1\ max}$ can be obtained from the geometry of Fig. 4.2

$$4.18 \quad y_{1\ max} \sin \theta_1 = \tan \eta_m (x \sec \rho_r + y_{1\ max} \cos \theta_1)$$

where η_m is the value of η obtained when y_2 lies along the edge of the receiver field of view (i.e. $\eta = \eta_m$ when $\rho' = \rho_r$). Solving Eq. 4.18 for $y_{1\ max}$ yields the following

$$4.18a \qquad y_{1\ max} = \frac{x \cdot \tan \eta_m}{\sin \theta - \cos \theta \cdot \tan \eta_m}$$

In order to obtain $y_{1\ max}$ from Eq. 4.18a an expression for η_m is required. Setting $\rho' = \rho_r$ in Fig. 4.2 and using the law of cosines for a spherical triangle yields:

$$4.19 \quad \cos \rho_r = \cos \eta_m \cdot \cos \rho + \sin \eta_m \cdot \sin \rho \cdot \cos \phi.$$

Substituting, $\sqrt{1-\sin^2\eta_m} = \cos\eta_m$, rearranging terms, squaring and applying the quadratic equation yields:

$$4.20 \quad \sin\eta_m = \frac{\sin\rho\cdot\cos\rho_r\cos\phi \pm \cos\rho\sqrt{1-\sin^2\rho\cdot\sin^2\phi-\cos^2\rho_r}}{1-\sin^2\rho\cdot\sin^2\phi}$$

The half-beam divergence angle ρ_L of most lasers is less than 2.5×10^{-3} radians while the half-angle divergence of the receiver field of view ρ_r is usually less than 5×10^{-3} radians. Therefore, because $\eta_m \leq \rho_L + \rho_r$ and $\rho \leq \rho_r$ small angle approximations can be used to express Eq. 4.20 as:

$$4.21 \quad \eta_m = \rho\cdot\cos\phi + \sqrt{\rho_r^2 - \rho^2\sin^2\phi}$$

The sign in front of the radical is positive because by definition η_m must always be positive. Application of the small angle approximation and the substitution of Eq. 4.21 into Eq. 4.18a yields:

$$4.22 \quad y_{1\,max} = \frac{x\cdot\left(\rho\cdot\cos\phi + \sqrt{\rho_r^2-\rho^2\cdot\sin^2\phi}\right)}{\sin\theta_1 - \cos\theta_1\cdot\left(\rho\cdot\cos\phi + \sqrt{\rho_r^2-\rho^2\cdot\sin^2\phi}\right)}$$

where $y_{1\,max}$ is the upper limit of integration for the y-integral in the basic double scatter equation (Eq. 4.17) when the y_1 distance is limited by the receiver field of view.

When a ray from S_1 in direction θ_1, ϕ is nearly parallel to the receiver axis it may not intersect the edge of the field of view. Inspection shows that whenever this occurs

the denominator of Eq. 4.22 is negative, therefore if

4.22a $\quad \sin \theta_1 \leq \cos \theta_1 \cdot \left(\rho \cos \phi + \sqrt{\rho_r^2 + \rho^2 \sin^2 \phi} \right)$

the upper limit of the y_1-integral

4.22b $\quad y_{1\ max} = \infty$.

A third expression for $y_{1\ max}$ occurs when a ray from S_1 in the direction θ_1, ϕ intersects the cloud base before intersecting the edge of the receiver field of view. This expression is obtained by considering the geometry of Fig. 4.1 in the special case where θ_1 is increased until the point S_2 is at the cloud base altitude x_c. The angle ρ is small (see the derivation of Eq. 4.20) therefore the cloud base can be considered perpendicular to the line $0, S_1$. With this simplification the geometry of triangle $0, S_1, S_2$ yields

4.22c $$y_{1\ max} = \frac{x \cdot \sec \rho - x_c}{-\cos \theta}$$

This is the correct upper limit for the y_1-integral whenever θ_1 is greater than $\pi/2$ and the distance to the cloud base (Eq. 4.22c) is less than the distance to the edge of the receiver field (Eq. 4.22).

4.4 Application of the propagation time-distance constraint

A photon transmitted at a time t' and received at time t must travel a total distance c(t-t'); in Eq. 4.17, this constraint on propagation distance is included in the transmitted power function. The temporal structure of the transmitted laser pulse can be separated from the interactions of system geometry and propagation delay effects if $\mathcal{G}_0(t-R/c)$ is rewritten with the aid of the Dirac delta function as follows:

$$4.23 \quad \mathcal{G}_0(t-R/c) = \int_0^{\Delta t} \mathcal{G}_0(t') \cdot \delta(t'-t+R/c) \, dt'$$

where Δt = **time** duration of the transmitted laser pulse

$\mathcal{G}_0(t')$ = transmitted power measured at the laser exit pupil

R = total path length = $X \cdot \sec \rho + y_1 + y_2$

Using this representation of the transmitted power the basic double scatter integral (Eq. 4.17) can be rewritten as

$$\mathcal{G}_2(t) = A \cdot \beta_s^2 \cdot \hat{u} \cdot \tilde{F} \cdot \int_0^{\Delta t} \mathcal{G}_0(t') \cdot dt' \int_0^{\rho_L} g(\rho) \cdot \tan\rho \, d\rho \int_0^{\pi} d\phi$$

$$4.24 \quad \cdot \int_{X_c}^{\infty} dX \int_0^{y_{1 max}} \frac{\delta(t'-t+R/c)}{y_2^2 \cdot 16\pi^2} \cdot e^{-\beta_E(R-X_c(\sec\rho+\sec\rho'))} \cdot dy_1$$

$$\cdot \int_0^{2\pi} \vec{S} \cdot d\xi$$

If $f(y)$ is an arbitrary function and a is an arbitrary constant, the delta function has the following properties:

4.25 $\quad \delta(f(y)) = \dfrac{1}{\left|\dfrac{df(y_{10})}{dy}\right|}\, \delta(y-y_{10}) \quad$ where $\quad f(y_{10})=0$

and

4.26 $\quad \displaystyle\int f(y)\cdot \delta(y-a)\cdot dy = f(a)$

With the aid of Eqs. 4.25 and 4.26 Eq. 4.24 can be expressed as:

4.27
$$\beta_z(t) = A\cdot \beta_s^2\,\hat{u}\cdot \tilde{F}\cdot c\cdot \int_0^{\Delta t}\beta_0(t')\cdot dt\int_0^{\rho_L} q(\rho)\cdot\tan\rho\, d\rho\int_0^{\pi}\sin\theta_1\, d\theta$$

$$\int_0^{2\pi} d\phi\int_{x_c}^{\infty}\frac{2\cdot e^{-\beta_E(L-x_c(\sec\rho+\sec\rho'))}}{|L^2+2(L\cos\theta_1)\cdot(x^2\sec^2\rho - L\cdot x\cdot\sec\rho)|}\cdot dx$$

$$\int_0^{y_{1,max}}\delta(y-y_0)\cdot dy\int_0^{2\pi}\vec{S}\cdot d\xi$$

Where R and $\displaystyle\int_0^{2\pi}\vec{S}\,d\xi$ are evaluated at the point t,t', ρ,θ_1,y_{10} and where R evaluated at the point (t,t') is identified as L. The values of L and y_{10} can be calculated from Eqs. 4.28 and 4.29.

4.28 $\quad L = c(t-t')$

4.29
$$y_{10} = \frac{L^2 - 2Lx\cdot\sec\rho}{2x\cdot\sec\rho\,\cos\theta_1 + 2L - 2x\cdot\sec\rho}$$

The y-integral of equation 4.27 can assume the following values

4.30 $\quad \displaystyle\int_0^{y_{1,max}}\delta(y_1 - y_{10})dy = 1 \quad$ if $0\le y_{10}\le y_{1,max}$

$\qquad\qquad$ " $\qquad\qquad = 0 \quad$ if $y_{10} < 0$

$\qquad\qquad$ " $\qquad\qquad = 0 \quad$ if $y_{10} > y_{1,max}$

Therefore, if new limits of integration are defined for the t',ρ,θ_1,ϕ and x integrals such that for all points inside the new integration volume $0 \le y_{10} \le y_{1\text{ max}}$, Eq. 4.30 can be applied to eliminate the y_1 integral. These new integration limits are simplified if values of the parameter t are restricted as follows

4.31
$$t \ge \frac{2\ x_c \cdot \sec\zeta_r}{c} + \Delta t.$$

The smallest values of t allowed by this expression can be interpreted as the earliest time at which photons from all portions of the transmitted laser pulse can contribute to the received signal. For typical lidar system parameters this minimum value of t occurs about 10^{-8} seconds after the first return is received from the cloud. Because most lidar receivers have a minimum time resolution on the order of 10^{-7} seconds condition 4.31 does not substantially reduce the generality of the double scatter equation.

An inspection of the equation for y_{10} (Eq. 4.39) shows that for any possible values of t',ρ,θ_1, and ϕ within the integration limits of Eq. 4.27 a value of x can be chosen such that $0 \le y_{10} \le y_{1\text{ max}}$. Thus, if condition 4.31 is satisfied only the x integration limits need modification to insure that Eq. 4.30 can be used to eliminate the y_1-integral. However, rather than calculate these new limits for the x-integral, the subsequent integration is simplified if the x-in-

tegral is first transformed into an integral in W, where W is given by

4.32 $W = L/2 - x \cdot \sec \rho$

This transformation allows 4.27 to be rewritten as:

$$4.33 \quad \beta_2(t) = A \cdot \beta_s^2 \cdot \hat{\omega} \cdot \tilde{F} \cdot 2 \cdot c \cdot \int_0^{\Delta t} \beta_0(t') \, dt' \int_0^{\rho_L} q(\rho) \sin \rho \, d\rho \int_0^{\pi} \sin \theta_1 \, d\theta_1$$

$$\int_0^{2\pi} d\phi \int_{W_\chi}^{W_\mu} \frac{-\int_0^{2\pi} S \cdot d\xi \cdot e^{-\beta_E (L - X_c \cdot (\sec \rho + \sec \rho'))}}{2 \cdot (1 - \cos \theta_1) \cdot W^2 + L^2/2 (1 + \cos \theta_1)} \cdot dW$$

Notice that L/2 is the maximum possible distance from the lidar system which a photon transmitted at t' can travel and still be received at time t. The variable W is therefore the distance from the first scattering event of a double scatter combination to the maximum possible distance L/2.

4.5 Integration limits for the W-integral

The limits of integration for the W-integral are the result of two separate constraints: 1) the first scattering event cannot occur below the cloud base because the scattering cross section per unit volume has been assumed to be zero outside of the cloud, and 2) according to Eq. 4.30

the distance from the first to the second scattering, y_1, must satisfy the condition $0 \leq y_{10} \leq y_{1\ max}$. A value for W_ℓ can be derived from the first constraint by substituting the cloud base altitude x_c into Eq. 4.32. This yields

4.34 $\quad W_\ell = L/2 - x_c \cdot \sec \rho$

$\qquad\qquad = L/2 - x_c.$

The W-limits required to satisfy the second constraint are now developed. As a first step in this development y_{10} (Eq. 4.29) is set to the extreme values allowed by Eq. 4.30. These equations are then transformed into equations in W with Eq. 4.34. The resulting expressions are solved for W_u and W_ℓ. From the equation $y_{10} = 0$, the following value is found for W_u.

4.35 $\quad W_u = 0.$

When $y_{10} = y_{1\ max}$ and $y_{1\ max}$ is determined by the edge of the receiver field of view, W_ℓ (Eq. 4.18a) becomes

4.36 $\quad W_\ell = \dfrac{L \tan(\gamma_r/2)}{2 \tan(\theta_r/2)}.$

When $y_{10} = y_{1\ max}$ is determined by the cloud base (Eq. 4.22a) W_ℓ is found to be

4.37 $\quad W_\ell = \frac{1}{2}\sqrt{x_c^2 + (L^2 - 2Lx_c)\cot^2(\theta/2)} - x_c/2.$

The upper limit of the W-integral is always given by Eq. 4.34. For the lower limit it is necessary to choose the smallest of equations 4.35, 4.36 or 4.37. By setting Eq. 4.34 equal to 4.36 and 4.36 equal to 4.37 the following conditions can be derived for the range of applicability of the W_ℓ expressions. The limit W_ℓ is given by Eq. 4.34 if $0 \leq \theta_1 \leq \theta_*$ where

$$4.38 \qquad \theta_* = 2 \cdot \tan^{-1}\left\{ \frac{L \cdot \tan(\eta_m/2)}{L - 2x_c} \right\}$$

If $\theta_* < \theta_1 < \theta_c$, W_ℓ is given by Eq. 4.36, where

$$4.39 \qquad \theta_c = 2 \cdot \tan^{-1}\left\{ \frac{L - x_c \cdot \sec \eta_m - x_c}{x_c \cdot \tan \eta_m} \right\}$$

and if $\theta_c \leq \theta_1 \leq \pi$, W_ℓ is given by Eq. 4.37.

4.6 Evaluation of the ξ-integral

Consider the ξ-integral of Eq. 4.33. The integrand $\vec{S}$ presented in Eq. 4.16 is a function of $\delta, \epsilon, \theta_2, \phi$ and θ_1. An inspection of Fig. 4.2 shows that δ, ϵ and θ_2 are functions of the independent variables x, ρ, θ_1, ϕ and y_1. Therefore, because they are not functionally dependent on ξ the ξ-integral can easily be evaluated

$$4.40 \quad \frac{1}{16\pi^2} \int_0^{2\pi} \vec{S} \cdot d\xi =$$

$$2\pi \left[P_1(\theta_2)\cdot P_1(\theta_1) + P_2(\theta_2)\cdot P_2(\theta_1) \right]$$

$$\frac{1}{16\pi^2} \begin{array}{l} \pi\cdot\cos 2(\phi-\phi') \\ \pi\cdot\sin 2(\phi-\phi') \end{array} \left[\begin{array}{l} P_2(\theta_2)\cdot P_2(\theta_1)+P_1(\theta_2)\cdot P_1(\theta_1) - P_3(\theta_2) P_3(\theta_1) + P_4(\theta_2) P_3(\theta_1) \\ \text{``} \qquad\qquad \text{``} \qquad\qquad\qquad \text{``} \qquad\qquad\qquad \text{``} \end{array} \right]$$

$$0$$

Equations for $\cos 2(\phi-\phi')$ and $\sin 2(\phi-\phi')$ will now be obtained. Applying the law of sines in a spherical triangle to Fig. 4.2 yields:

$$4.41 \qquad \sin\gamma = \frac{\sin\rho\cdot\sin\phi}{\sin\rho'}$$

and

$$4.42 \qquad \sin\varepsilon = \frac{\sin\eta\cdot\sin\phi}{\sin\rho'}$$

where

$$4.43 \quad \eta\simeq\sin\eta \quad \frac{y_1\cdot\sin\theta_1}{\sqrt{(x\cdot\sec\rho + y_1\cdot\cos\theta_1)^2 + y_1{}^2\sin^2\theta_1}}$$

is obtained from the geometry of the plane triangle $0,S,S_2$. From the law of cosines in a spherical triangle:

$$4.44 \qquad \cos\phi = -\cos\gamma\cos\varepsilon + \sin\gamma\sin\varepsilon\cos\rho'.$$

Because $\rho'\leqslant\rho_r\leqslant 5\times 10^{-3}$, $\cos\rho'\simeq 1 - \rho'^2/2$. With the aid of the identity for the cosine of the sum of angles this approximation can be applied to 4.44 yielding:

4.45 $\cos\phi = -\cos(\gamma+\epsilon) - \dfrac{\rho'^2 \sin\gamma \sin\epsilon}{2}$

From definition 4.15

4.46 $-\cos(\gamma+\epsilon) = \cos(\pi-\gamma-\epsilon) = \cos\phi'$.

Substituting Eqs. 4.41, 4.42, and 4.46 into 4.45 and then applying the small angle approximation (because $\eta\rho \ll 1$) yields:

4.47 $\cos\phi' \approx \cos\phi + \dfrac{\eta\cdot\rho}{2}\sin^2\phi$

This equation and the following double angle identity

4.48 $\cos 2\phi' = 2\cos^2\phi' - 1$

yield, after dropping terms in $\eta^2\rho^2$:

4.49 $\cos 2\phi' = \cos 2\phi + 2\eta\rho\cos\phi\sin^2\phi$.

Eq. 4.47 and the double angle identity,

4.50 $\sin 2\phi' = 2\cdot\cos\phi'\sqrt{1-\cos^2\phi'}$

lead to the following:

4.51 $\sin 2\phi' = 2(\cos\phi + \dfrac{\eta\cdot\rho}{2}\sin^2\phi)$

$$\sqrt{1 - \cos^2\phi + \eta\cdot\rho\cos\phi\sin^2\phi + \dfrac{\eta^2\rho^2\cdot\sin^4\phi}{4}}$$

Neglecting terms in $\eta^2\rho^2$ and expanding the square root,

4.52 $\sin 2\phi' = \sin 2\phi - \eta\rho\sin\phi\cos 2\phi$

The identity for the sine of a sum of angles,

4.53 $\sin(2\phi-2\phi') = \sin 2\phi\cos 2\phi' - \cos 2\phi\sin 2\phi'$,

along with Eqs. 4.49 and 4.52 provide an equation for one of the terms appearing in Eq. 4.40:

4.54 $\sin 2(\phi-\phi') = \eta\rho\sin\phi$

The cosine term appearing in the third component of $\int_0^{2\pi}\vec{S}\cdot d\xi$ (Eq. 4.17) can be derived from the identity

4.55 $\cos 2(\phi-\phi') = \sqrt{1 - \sin^2 2(\phi-\phi')}$.

Substituting 4.54 into this equation yields:

4.56 $\cos 2(\phi-\phi') = \sqrt{1 - \eta^2\rho^2\sin^2\phi}$.

However since $\rho \leq 2.5 \times 10^{-3}$ radians Eq. 4.56 can be written to a very good approximation as:

4.57 $\cos 2(\phi-\phi') \cong 1$

With the aid of Eqs. 4.54 and 4.57 the $\cos 2(\phi-\phi')$ and the $\sin 2(\phi-\phi')$ terms of the ξ-integral (Eq. 4.40) can be expressed in terms of the independent variable ϕ. Before attempting to evaluate the W-integral the dependent variable

θ_2 must also be expressed in terms of the independent variables. Simple geometry applied to triangle O, S_1, S_2 of Fig. 4.1 indicates that:

4.58 $\qquad \theta_2 = \pi - \theta_1 + \eta$

Because $\eta \le \rho_r + \rho_L$ it is clear that η is a small angle. In the typical lidar system where $\rho_L \le 2.5 \times 10^{-3}$ and $\rho_r \le 5 \times 10^{-3}$ rad., $\eta \le 7.5 \times 10^{-3}$ rad. A considerable simplification to Eq. 4.33 can be obtained at the expense of a loss of some accuracy by introducing the approximation:

4.59 $\qquad \theta_2 \approx \pi - \theta_1$

The error introduced by this approximation will be estimated in section 6.

4.7 Evaluation of the W-integral

As a first step in the evaluation of the W-integral, the attenuation term of E. 4.33 can be simplified with the small angle approximation for the secant as follows:

4.60 $\qquad e^{-\beta_E \left(L - x_c \left(\sec \rho + \sec \rho' \right) \right)}$

$$\approx e^{-\beta_E \left(L - 2 x_c \right)} \cdot e^{\beta_E \cdot x_c \left(\rho'^2/_2 + \rho^2/_2 \right)}$$

Using values of cloud height for a high cloud ($x_c = 10^4$ m) with a large extinction coefficient ($\beta_E = 0.1$ m^{-1}) the largest value of $\beta_E \cdot x_c \cdot (\rho'^2/2 + \rho^2/2)$ likely to be encountered can be estimated. For $\rho \leq \rho_L \leq 25 \times 10^{-3}$ radian and $\rho' \leq \rho_r \leq 5 \times 10^{-3}$ radian

4.61 $\quad e^{\beta_E \cdot x_c \cdot (\rho'^2/2 + \rho^2/2)} \leq e^{.015} \cong 1 + .015$

It is therefore reasonable to introduce the following approximation into Eq. 4.33

4.62 $\quad e^{-\beta_E \cdot (L - x_c \cdot (\sec \rho + \sec \rho'))} \cong e^{-\beta_E (L - 2x_c)}$.

As a second step in the evaluation of the W-integral expressions 4.54, 4.57 and 4.59 are used to simplify the Stokes vector resulting from the ξ-integration (Eq. 4.40). The first two components of the resulting vector are independent of both W and ϕ. The third component is an antisymmetric function of ϕ about $\phi = 0$ and the W integral of Eq. 4.33 is independent of ϕ except for W_ℓ which is symmetric in ϕ about $\phi = 0$. Therefore, integration over W and ϕ eliminates the third component of Eq. 4.40. Because this entire vector is now independent of both W and ϕ it can be moved to the θ_1-integral.

Thus if the approximate form of the extinction term presented in Eq. 4.62 is introduced, the double scatter integral can be reduced to the following form

$$4.63 \quad \vec{Q}_2(t) = A \cdot \beta_s^2 \cdot \hat{u} \cdot \tilde{F} \cdot 2 \cdot c \cdot \int_0^{\Delta t} \vec{Q}_0(t) \cdot e^{-\beta_E(L - 2 X_c)} dt' \int_0^{\rho_L} q(\rho) \cdot \sin\rho \cdot d\rho$$

$$\int_0^{\pi} \sin\theta_1 \cdot \vec{S}'(\theta_1) \cdot d\theta_1 \int_0^{2\pi} d\phi \int_{W_\ell}^{0} \frac{-2 \cdot dW}{4(1-\cos\theta) \cdot W^2 \cdot L^2 \cdot (1+\cos\theta)}$$

where

$$4.64 \quad \vec{S}'(\theta_1) =$$

$$\frac{1}{16\pi^2} \begin{pmatrix} 2\pi \left[P_1(\pi-\theta_1) \cdot P_1(\theta_1) + P_2(\pi-\theta_1) \cdot P_2(\theta_1) \right] \\ \pi \left[P_1(\pi-\theta_1) \cdot P_1(\theta_1) + P_2(\pi-\theta_1) \cdot P_2(\theta_1) - P_3(\pi-\theta_1) \cdot P_3(\theta_1) + P_4(\pi-\theta_1) \cdot P_4(\theta_1) \right] \\ 0 \\ 0 \end{pmatrix}$$

The W-integral of Eq. 4.63 can be integrated by standard techniques, which yield:

$$4.65 \quad -\int_{W_\ell}^{0} \frac{2 \cdot dW}{4(1-\cos\theta_1) \cdot W^2 + L^2(1+\cos\theta_1)} = \left(\frac{1}{L \cdot \sin\theta_1}\right) \cdot \tan^{-1} \left\{ \frac{2 \cdot W_\ell}{L} \cdot \tan\left(\frac{\theta_1}{2}\right) \right\}$$

Applying this result to Eq. 4.63 yields the following equation for doubly scattered power:

$$4.66 \quad \boxed{\vec{Q}_2(t) = c \cdot A \cdot \beta_s^2 \cdot \hat{u} \cdot \tilde{F} \int_0^{\Delta t} \vec{Q}_0(t') \cdot e^{-\beta_E(L-2 X_c)} \cdot \vec{G}(t, t') \cdot dt'}$$

where the Stokes vector impulse transfer function $\vec{G}(t,t')$ is defined as follows:

$$G(t,t') = \frac{2}{L} \cdot \int_0^\pi \vec{S}'(\theta_1) \cdot d\theta_1 \int_0^{\rho_L} g(\rho) \rho \, d\rho \cdot$$
$$\int_0^{2\pi} \tan^{-1}\left\{ \left(\frac{2 \cdot W \iota}{L}\right) \cdot \tan\left(\frac{\theta_1}{2}\right) \right\} d\phi$$

4.67

For ease of reference the variables used in these two equations are redefined below

$L = c(t-t')$ = total path length

c = speed of light

t = time

A = receiver area

β_s = scattering cross section per unit volume

β_E = extinction cross section per unit volume

$\hat{u}$ = (1,0,0,0) = a unit Stokes vector

$\tilde{F}$ = Mueller matrix describing the polarizing filter on the receiver

β_0 = transmitted power

x_c = cloud base altitude

ρ_L = half angle divergence of the cone containing all the transmitted energy

$g(\rho)$ = relative angular distribution function for transmitted energy (see condition 4.2)

θ_1 = angular deflection of the first scattering event (Figs. 4.1 and 4.2)

ρ = angular displacement from system axis (Figs. 4.1 & 4.2)

ϕ , see Figs. 4.1 and 4.2

S', see Eq. 4.64

$^W\ell$, see Eqs. 4.34 through 4.39.

The transfer function presented in Eqs. 4.66 and 4.67 predicts both the magnitude and the polarization of the doubly scattered component of a lidar return from a homogeneous cloud. This fundamental equation serves as the basis for the remainder of this paper; in later sections it will be written in simplified versions for special cases and also evaluated numerically for several cloud models.

5. THE DOUBLE SCATTER TRANSFER FUNCTION IN SPECIAL CASES

In this section the fundamental double scatter transfer function (Eq. 4.66) is presented in simplified form for several special cases. Of particular interest is the special form which results when the scattering matrix element $P_1(\theta)$ has a Gaussian angular dependence at small angles. In this case the doubly scattered signal can be evaluated without recourse to cumbersome numerical integrations.

5.1 Lidar systems transmitting short pulses

In the limit where the pulse duration Δt of the transmitting laser approaches zero and when the laser pulse is transmitted at time $t = 0$; evaluation of the t' integral in Eq. 4.66 yields:

$$5.1 \quad \overrightarrow{G}_2(t) = E_0 \cdot c \cdot A \cdot \beta^2 \cdot \hat{u} \cdot \tilde{F} \; \overrightarrow{G}(t,0) \; e^{-2\beta d}$$

where $d = (ct - x_c)/2$ and
the time integral of the transmitted power is identified as the transmitted energy E_0. The optical pulses transmitted by most lidar systems are on the order of 10^{-8} seconds long; however, the receiver electronics on these systems usually integrate the received signal over time period on the order of 10^{-7} seconds. Because the receiver integration time is 10 times Δt, the time integral included in Eq. 4.66 has little effect on the observed signal. Thus for most lidar

CORRECTION

$$d = \frac{ct}{2} - x_c$$

systems it is not necessary to perform the integration included in Eq. 4.66. The results obtained from Eq. 5.1 can simply be averaged over the receiver response time to calculate the doubly scattered return.

5.2 Unpolarized receiver -- short transmitted pulse

The Mueller matrix $\widetilde{F}$ contained in Eqs. 4.66 and 5.1 makes it possible to calculate the doubly scattered power detected by a receiver equiped with any type of polarizing filter. It is instructive to consider the form of Eq. 5.1 in the special case where the receiver is unpolarized. In this case the Mueller matrix $\widetilde{F}$ is given by

$$5.2 \qquad \widetilde{F} = \begin{pmatrix} 1 & 0 & 0 & 0 \\ 0 & 1 & 0 & 0 \\ 0 & 0 & 1 & 0 \\ 0 & 0 & 0 & 1 \end{pmatrix}$$

and Eq. 5.1 can be written

$$5.3 \qquad Q_2(t) = E_0 \cdot A \cdot c \cdot \beta^2 \cdot G_I(t,0) \cdot e^{-2\beta d}$$

where $G_I(t,0)$ = the first component of the vector $\overrightarrow{G}(t,0)$ derived from Eq. 4.67.

5.3 Linearly polarized receiver -- short transmitted pulse

The Mueller matrix $\widetilde{F}$ for a linearly polarized receiver

arranged such that the transmission direction of the polar-
izing filter is oriented at an angle ζ with respect to the
polarization direction of the transmitted energy is given
by

$$5.4 \qquad \underset{\sim}{F} = 1/2 \begin{pmatrix} 1 & \cos 2\zeta & \sin 2\zeta & 0 \\ \cos 2\zeta & \cos^2 2\zeta & \cos 2\zeta \sin 2\zeta & 0 \\ \sin 2\zeta & \cos 2\zeta \sin 2\zeta & \sin^2 2\zeta & 0 \\ 0 & 0 & 0 & 0 \end{pmatrix}$$

and the double scatter equation becomes

$$5.5 \quad G_2(t) = \tfrac{1}{2} E_o \cdot A \cdot c \cdot \beta^2 e^{-2\beta d} \cdot \left\{ G_I(t,0) + \cos(2\zeta) \cdot G_Q(t,0) \right\}$$

where G_Q is the second component of the vector $\vec{G}(t,0)$

5.4 Transmitter with small angular divergence — short
   transmitted pulse

As the laser beam divergence approaches zero, the angu-
lar distribution function $g(\rho)$ approaches the Dirac delta
function form

$$5.6 \qquad g(\rho) = \tfrac{1}{2\pi} \cdot \delta(\rho)$$

Using this form of g, the ρ-integral of the vector transfer
function (Eq. 4.67) can be integrated directly. The integra-
ted function, which includes W_ρ (Eq. 4.34, 4.36 and 4.37)
evaluated at $\rho = 0$, is independent of ϕ; therefore, the

ϕ-integral can be reduced to a multiplication by 2π. These integrations yield the following small beam divergence form of the vector impulse transfer function

$$5.7 \quad \vec{G}(t,t') = \frac{1}{L} \int_0^\pi \vec{S'}(\theta_1) \cdot \tan^{-1}\left[\frac{2 \cdot W_\ell}{L} \cdot \tan(\theta_1/2)\right] \cdot d\theta_1$$

The function W_ℓ is evaluated at $\rho = 0$ and is selected according to the criteria listed in section 4 from the set of Eqs. 4.34, 4.36 and 4.37.

5.5 Gaussian forward scattering peak -- small transmitter divergence -- short transmitted pulse

In Appendix A, it is shown that for some water droplet size distributions, the small angle forward scattering has a nearly Gaussian angular dependence. In this case further simplification of the small beam divergence impulse transfer function (Eq. 5.7) is possible. The approximate relationship is obtained when a Gaussian diffraction peak is introduced into the scattering matrix as follows

$$5.8 \quad P_1(\theta) = P_1(0) \cdot \exp\left\{-\theta^2/\langle\theta^2\rangle\right\} \qquad \theta \le \pi/2$$

where $P_1(0)$ = actual value of the scattering matrix element $P_1(\theta)$ evaluated at $\theta = 0$

$\langle\theta^2\rangle$ = mean square angle of scattering for small angle scattering $\sqrt{\dfrac{1}{2\pi \cdot P_1(0)}}$ (Appendix A)

and where for $\theta \geq \pi/2$ $P_1(\theta)$ is given by the actual values of the matrix element. With this approximation the first component of the vector $\vec{G}$ defined by Eq. 5.7 becomes

5.9 $\quad G_I = \dfrac{2\pi \cdot P_1(0)}{L} \displaystyle\int_0^\infty P_1(\pi - \theta_1) \cdot e^{-\theta^2/\langle\theta^2\rangle} \cdot \tan^{-1}\left\{\dfrac{2 \cdot W_l}{L} \cdot \tan(\theta/2)\right\} \cdot d\theta_1$

$\quad + \dfrac{2\pi \cdot P_1(0)}{L} \displaystyle\int_0^\infty P_1(\pi - \theta_1) \cdot e^{-\theta^2/\langle\theta^2\rangle} \cdot \tan^{-1}\left\{\dfrac{2 \cdot W_l}{L} \cdot \tan\left(\dfrac{\pi - \theta_1}{2}\right)\right\} \cdot d\theta_1$

Notice that the vector $\vec{G}'$ contained in Eq. 5.7 has been simplified by neglecting the $P_2(\theta_1)$ $P_2(\pi - \theta_1)$ contribution to the doubly scattered return. The validity of this assumption can be verified by inspection of the matrix elements presented in Appendix A.

In Eq. 5.9 the doubly scattered contribution is divided into two separate terms; these terms reflect the order in which the scattering events occurred. Doubly scattered photons contributing to the first term are scattered first through a small forward angle and then turned back toward the receiver by a deflection of nearly π radians. The second term represents the contribution due to photons which first undergo a large angle scattering and then a small angle event.

The diffraction peak concentrates scattered light into a narrow angular cone; small angle approximations may therefore be used to simplify Eq. 5.9. When these approximations are applied, after substituting Eqs. 4.34, 4.36 and 4.37 for

$W_{\mathfrak{l}}$, the following expression results

$$G_I = \frac{1/2 \pi}{L} \cdot \frac{P_1(0)}{4\pi} \cdot \int_0^{\theta_*} \frac{P_1(\pi - \theta_1)}{4\pi} \cdot e^{-\theta_1^2/\langle\theta^2\rangle} \cdot \theta_1 \, d\theta_1$$

5.10

$$+ \frac{2\pi P_1(0)}{2 \cdot L \cdot X_c \cdot 4\pi} \int_0^{\theta_c} \frac{P_1(\pi - \theta_1)}{4\pi} e^{-\theta_1^2/\langle\theta^2\rangle} \cdot \theta_1 \, d\theta_1$$

$$+ \frac{2\pi P_r P_1(0)}{L} \cdot \frac{P_1(0)}{4\pi} \cdot \int_{\theta_c}^{\infty} \frac{P_1(\pi - \theta_1)}{4\pi} e^{-\theta_1^2/\langle\theta^2\rangle} \cdot d\theta_1$$

$$+ \frac{1/2 \pi P_r}{L} \cdot \frac{P_1(0)}{4\pi} \cdot \int_{\theta_*}^{\infty} \frac{P_1(\pi - \theta_1)}{4\pi} e^{-\theta_1^2/\langle\theta^2\rangle} \cdot d\theta_1$$

where θ_* = the angle at which the expression for W_i

changes from Eq. 4.34 to 4.36

$\theta_* \cong L \, \rho_r/2d$

θ_c = the angle defined by Eq. 4.39

$\theta_c \cong \rho_r x_c/d + \rho_r = \theta_*$

ρ_r = receiver half-angle acceptance cone

$d = (L - 2x_c)/2$ cloud penetration depth

x_c = cloud base altitude

$P_1(0)$ = scattering matrix element $P_1(\theta)$ evaluated at

$\theta = 0$

If the mean value theorem is used to remove the average value of $P_1(\pi - \theta_1)$ from the integrals above, the first two terms can be integrated by standard techniques and the second two terms can be identified as error functions. If this were to be an exact evaluation of the above integrals, a different value for the average $\langle P_1(\pi)\rangle_2$ should be derived for each integral as a function of the integration limits; however, this average is a realatively insensitive function

of the integration limits and can be estimated with
Eq. 3.11. With this approximation Eq. 5.10 can be reduced
to the following simple form

5.11
$$G_I = \frac{2d}{L^2} \cdot \frac{\langle P_i(\pi)\rangle_2}{4\pi} \cdot \left[1 - \exp\left\{-\frac{L^2 \cdot \rho_r^2}{4d^2 \langle \theta^2\rangle}\right\}\right]$$
$$+ \frac{d}{2L} \frac{\langle P_i(\pi)\rangle_2}{x_c} \cdot \frac{\langle P_i(\pi)\rangle_2}{4\pi} \left[1 - \exp\left\{-\frac{x_c^2 \rho_r^2}{d^2 \langle \theta^2\rangle}\right\}\right]$$
$$+ \frac{1}{2} \frac{\rho_r}{L} \cdot \frac{\langle P(\pi)\rangle_2}{4\pi} \sqrt{\frac{\pi}{\langle\theta^2\rangle}} \left[1 - erf\left\{\frac{\rho_r \cdot x_c}{d \cdot \sqrt{\langle\theta^2\rangle}}\right\}\right]$$
$$+ \frac{1}{2} \frac{\rho_r}{L} \cdot \frac{\langle P_i(\pi)\rangle_2}{4\pi} \sqrt{\frac{\pi}{\langle\theta^2\rangle}} \cdot \left[1 - erf\left\{\frac{\rho_r \cdot L}{2d\sqrt{\langle\theta^2\rangle}}\right\}\right]$$

see page

where the error function evaluated at a point Z is given by

5.12
$$erf(Z) = \frac{2}{\sqrt{\pi}} \int_0^z e^{-t^2} dt$$

and the approximate relationship

5.13
$$2\cdot\pi \cdot \frac{P_i(0)}{4\pi} \cdot \langle\theta^2\rangle = 1$$

has been introduced (see Appendix A for a derivation of 5.13).

The terms of Eq. 5.11 are presented in the same order as
they were written in Eq. 5.10; thus the first term can be
identified as the doubly scattered contribution due to all
scattering when the first scattering involves an angular
deflection θ_1 in the range $0 \le \theta_1 \le \frac{L \rho_r}{2d}$. The second gives
the contribution due to the angular range $\pi - \frac{\rho_r \cdot x_c}{d} \le \theta_1 \le \pi$ while
the third and fourth terms account for scattering with

$$\frac{L-\rho_r}{2d} \leq \theta_1 \leq \pi - \frac{\rho_r x_c}{d} \quad .$$

Although Eq. 5.11 contains a relatively large number of approximations it is, because of its simplicity, perhaps the most useful result of the present paper. A comparison of the G_I's calculated from 5.11 and those from the exact form presented in Eq. 4.67 is presented in section 6. In the cases examined, Eq. 5.11 is shown to provide a good approximation to the exact form.

When a lidar return is to be analyzed with the single scatter equation, contributions to the signal due to double scattering may introduce substantial error. Part of the usefulness of Eq. 5.11 lies in the ease with which it can be applied to estimate the magnitude of this error. Consider for example, the lidar return observed when the system is immersed in a hazy atmosphere. In this case, where the cloud base altitude x_c is zero and the r.m.s. diffraction peak scattering angle $\sqrt{\langle\theta^2\rangle}$ is much larger than the angular field of view*, $2\rho_r$ Eq. 5.11 reduces to

$$5.14 \qquad G_I = \frac{\rho_r}{L} \cdot \frac{\langle P_1(\pi)\rangle_2}{4\pi} \cdot \sqrt{\frac{\pi}{\langle\theta^2\rangle}}$$

---

*See appendix A for examples of the scattering matrix for model haze particle size distributions. Although the assumption of a Gaussian diffraction peak is less satisfactory for the haze models than it is for the cloud size distributions the comparisons presented in section 6 show that reasonable estimates are possible with Eq. 5.15.

because $\rho_r \ll \sqrt{\langle\theta^2\rangle}$ terms in $\rho_r^2/\langle\theta^2\rangle$ have been assumed negligible in comparison to $\rho_r/\sqrt{\langle\theta^2\rangle}$. This equation can then be substituted into 5.3 to give the doubly scattered power received by a non-polarized receiver. If the resulting expression is divided by the single scatter lidar equation the ratio of double to single scattering can be estimated. This ratio is given by

$$5.15 \qquad \beta_2/\beta_1 \approx \sqrt{\pi} \cdot \beta_s \cdot \frac{L}{2} \cdot \left(\frac{\rho_r}{\sqrt{\langle\theta^2\rangle}}\right)$$

Because the haze size distributions tend to have little variation in $P_1(\theta_1)$ near the backscatter direction (Appendix A) the ratio $\frac{\langle P_1(\pi)\rangle_\lambda}{P_1(\pi)}$ has been set equal to 1 in the derivation of Eq. 5.15.

Additional physical insight is provided by comparing this equation to the small penetration depth approximation for β_2/β_1 developed in section 3 (Eq. 3.11). When the cloud base altitude $x_c = 0$ the penetration depth $d = L/2$. Therefore, when it is assumed $\frac{\langle P_1(\pi)\rangle_\lambda}{P_1(\pi)} = 1$, Eq. 5.15 and Eq. 3.11 differ only by a factor $\sqrt{\pi} \cdot \left(\frac{\rho_r}{\sqrt{\langle\theta^2\rangle}}\right)$. This factor clearly represents the fraction of the small angle forward scattering which is scattered out of the receiver field of view. Notice that as the r.m.s. width of the forward scattering peak $\sqrt{\langle\theta^2\rangle}$ becomes larger more energy is scattered out of the receiver field of view and the ratio β_2/β_1 becomes smaller.

The double scatter transfer function (Eq. 4.66) from which equation 5.15 was derived is based on the assumption of a homogeneous scattering medium. However, Eq. 5.15 is applicable to a more general case where the haze is not homogeneous. From propagation time considerations and the small angle approximation it is known that one of the pair of scatterings making up a double scatter event occurs at a distance L/2 from the lidar. This scattering provides a deflection of nearly π radians. The other scattering must produce a small deflection. Notice that if this small angle scattering deflects the photon by an angle θ_1 the event must occur within the interval between $\frac{L}{2}(1 - \frac{\rho_r}{\theta_1})$ and L/2, otherwise the radial component of the photon's motion will carry it out of the receiver field of view. Examination of Eq. 5.10 along with a tabulation of the error function shows that if all photons deflected less than $0.18\sqrt{\langle\theta^2\rangle}$ radians are neglected only 20% of the power contributing to Eq. 5.15 is lost. Therefore 80% of the doubly scattered energy must result from combinations of scattering events occuring within the interval between $\frac{L}{2}(1 - \frac{\rho_r}{0.18\sqrt{\langle\theta^2\rangle}})$ and L/2. As long as the value of β_s and/or $\frac{\rho_r}{\sqrt{\langle\theta^2\rangle}}$ is not decreasing in such a way that lower levels make an inordinate contribution to the doubly scattered signal, the homogeneity requirement on 5.15 applies only to this more limited range interval.

Rough estimates of the parameters included in Eq. 5.15 will now be used to obtain estimates of the double to single

scatter ratios. First consider the lidar return from a range of 10 km in a moderate haze ($\beta = 0.2$ km^{-1}) with a size distribution given by the haze C model presented in Appendix A. If the receiver angular field of view $2\rho_r = 10^{-2}$ radians, the double to single scatter ratio for this case is

$$5.16 \quad \beta_2/\beta_1 \approx (1.7) \cdot (0.2 \text{ km}^{-1}) \cdot (10 \text{ Km}) \cdot \left(\frac{5 \times 10^{-3}}{3.5 \times 10^{-2}} \right)$$
$$\approx 8\%$$

Now consider a light fog ($\beta = 1$ km^{-1}) with a size distribution given by cloud model C-1. If the same receiver is used and the observation distance is 1 km,

$$5.17 \quad \beta_2/\beta_1 \approx (1.7) \cdot (1 \text{ km}^{-1}) \cdot (1 \text{ km}) \cdot \left(\frac{5 \times 10^{-3}}{3.5 \times 10^{-2}} \right)$$
$$\approx 25\%$$

These estimates indicate that the doubly scattered contribution to a lidar return cannot automatically be considered negligible even when the return does not involve penetration into an optically dense cloud.

6. NUMERICAL COMPUTATIONAL METHODS AND ERROR ESTIMATES FOR THE GENERAL DOUBLE SCATTER TRANSFER FUNCTION

Evaluation of the exact vector impulse transfer function (Eq. 4.67) must be performed by means of numerical integration. This section describes the integration scheme used in the present analysis. The errors introduced by this quadrature along with the errors due to the θ_2-approximation (see section 4) are also discussed.

6.1 The numerical integration scheme

In this development, values of the vector impulse transfer function for double scattering were obtained with a Simpson's rule quadrature. A computer program was written to estimate numerically the integral of an arbitrary function on a specified interval. This routine proceeds by interval halving as follows:

i) The function is evaluated at the endpoints and the center of the interval. An estimate of the integral is then made with a standard 3-point Simpson's rule quadrature.

ii) The distance between each previous function evaluation is identified as a new sub-interval. The function is evaluated at the mid-points of each of these sub-intervals and Simpson's rule applied to each.

iii) The fractional change f between this new estimate

of the integral, ϑ_n, and the previous estimate, ϑ_{n-1}, is then calculated as follows:

$$f = \left| \frac{\vartheta_n - \vartheta_{n-1}}{\vartheta_n} \right|$$

6.1

If f is smaller than a preselected convergence criterion ϵ the last estimate ϑ_n is accepted as the value of the integral. If $f > \epsilon$ the intervals are subdivided again as in step ii and the procedure is repeated until $f \leq \epsilon$.

The ϕ-integral in Eq. 4.67 is evaluated by a computer routine of this type. This routine is nested in a similar program element which calculates the ρ-integral. Because the Θ_1-integration must be performed on a two component vector, the quadrature discussed above was modified to accept a second component. In the modified version interval halving is carried out until both components of the integrated vector meet the convergence criterion.

Because the functions $\vec{S}(\Theta_1)$ and $\tan (\Theta_1/2)$ vary rapidly for Θ_1 near 0 and π the Θ_1-integral was subdivided into three intervals (0 to 0.2 rad., 0.2 to 2.94 rad., and 2.94 to π rad.). This subdivision substantially speeds convergence of the Θ_1 integrations. Notice that even though $\tan(\frac{\Theta_1}{2})$ becomes infinite at $\Theta_1 = \pi$ the integrand is finite because W_Q approaches zero at π.

6.2 Tests of integral convergence

The numerical quadrature described above generates an

approximate value G_n for the integral $G(t,t')$ presented in Eq. 4.67. The accuracy of this quadrature depends on the functional behavior of the integrand and the value selected for the convergence parameter ϵ; thus, $G(t,t') \approx G_n(t,t',\epsilon)$. The dependence of G_n on ϵ was investigated by computing G_n for several values of ϵ. Figs. 6.1 and 6.2 show examples of this dependence plotted in terms of the approximate fractional quadrature errors F_I and F_Q, where

$$F_{I,Q}(\epsilon) = \frac{G_{I,Q}(t,t',\epsilon) - G_{I,Q}(t,t',0.0025)}{G_{I,Q}(t,t',0.0025)} \qquad 6.2$$

and G_I = first component of the vector $\vec{G}_n$

G_Q = second component of the vector $\vec{G}_n$.

Notice that F_I and F_Q are approximations to the fractional error because the exact values of the vector components are not available and can only be estimated by applying the quadrature with a small ϵ (in this case with $\epsilon = 0.0025$). The time required for evaluation of G_n on a Univac 1108 computer is also plotted in Figs. 6.1 and 6.2. The lidar systems parameters used in these calculations are the same as those used for the results presented in Fig. 7.1. Fig. 6.1 assumes a homogeneous cloud with a size distribution given by Deirmendjian's cloud model C-1 and a cloud base altitude of 1 km. In Fig. 6.2 cloud model C-4 is assumed with a 1 km. cloud base. Both sets of calculations were performed for the case $t-t' = 7.66 \times 10^{-6}$ sec. (i.e. a 120 m cloud penetration
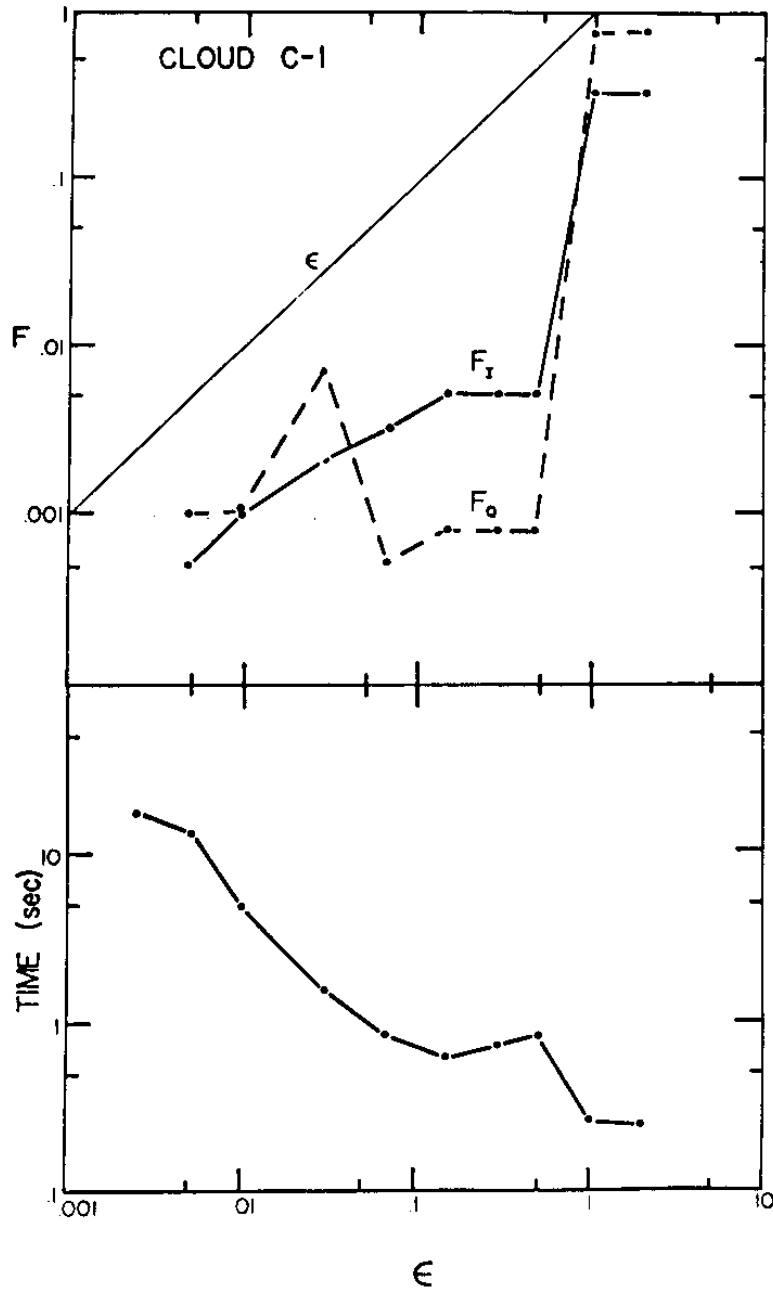
Fig. 6.1 Fractional quadrature errors in $G_I(\epsilon)$ and $G_Q(\epsilon)$
(Eq. 6.2) and computation time for $\overline{G}_n(\epsilon)$. These computa-
tions assume: cloud model C-1, cloud base altitude x_c = 1 km,
receiver field of view $2\rho_r$ = 0.004 rad., laser beam diver-
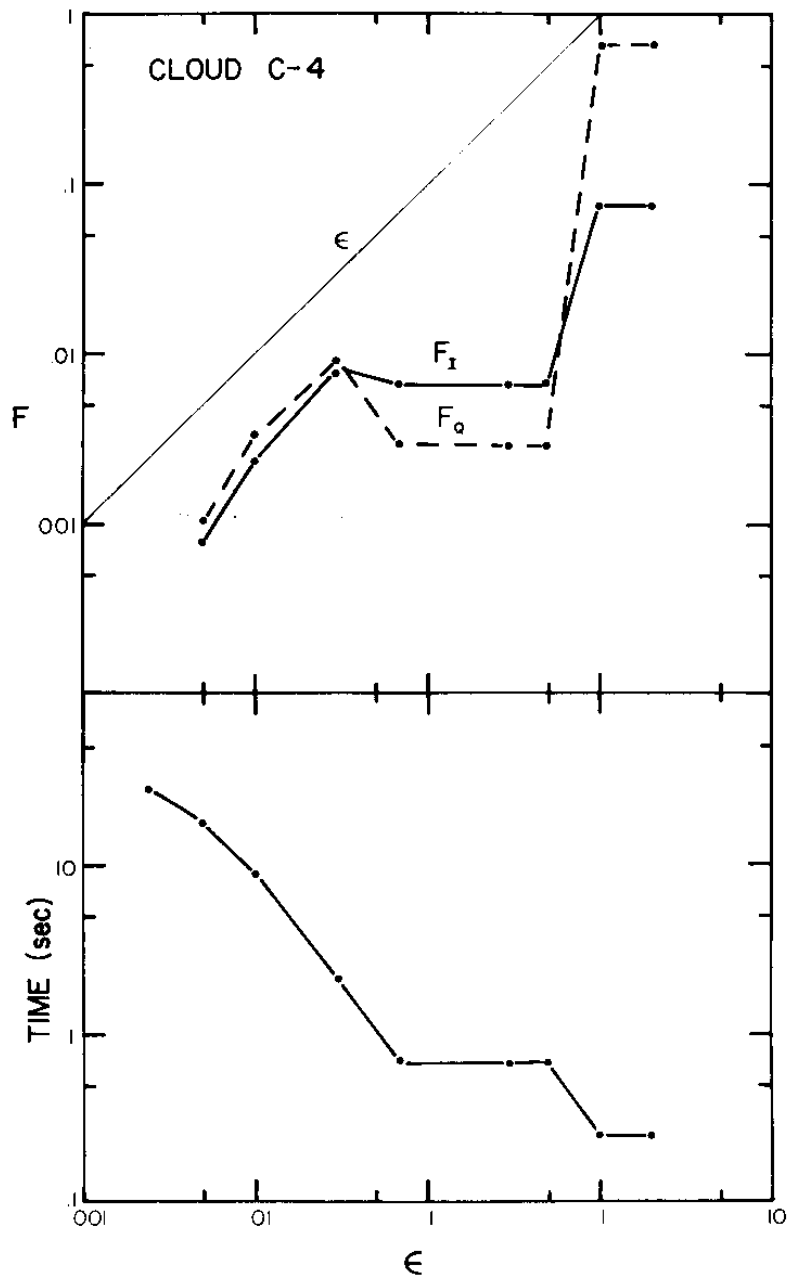gence $2\rho_L$ = 0.002 rad. laser energy distribution given by
(Eq. 6.6).

Fig. 6.2 Fractional quadrature errors and computation time for $G_n(\epsilon)$. These compuations are for cloud C-4. All other parameters are the same as in Fig. 6.1.

depth).

The curves plotted in Figs. 6.1 and 6.2 show that it is reasonable to assume that the fractional error introduced by the quadrature is less than ϵ . These curves also indicate that the choice of ϵ involves a compromise between computational accuracy and the computation time. Notice that the convergence properties are similar for cloud models C-1 and C-4 even though the angular variation of the off-diagonal elements P_2 and P_4 of the scattering matrix are considerably more complex in the C-4 case. This added complexity introduces only slightly slower convergence rates and small increases in computation time.

Unless otherwise noted calculations presented in the remainder of this paper will assume $\epsilon = 0.05$ for all integration A quadrature introduced error of less than 5% is therefore expected in the calculated components of $\vec{G}(t,t')$. The results presented in Figs. 6.1 and 6.2 indicate that this error may frequently be less than 1%.

6.3 Effects of the θ_2-approximation

The double scatter equation was considerably simplified by the introduction of an approximate value for the second scattering angle θ_2. This approximation, contained in Eq. 4.62, sets the angle $\eta = 0$. The actual value of η for any

pair of scattering events is given by Eq. 4.49 and falls in
the range:

$$0 \le \eta \le \rho_L + \rho_r \qquad\qquad 6.3$$

The approximate values of Θ_2 derived from Eq. 4.62 consis-
tently underestimate the actual values of Θ_2.

In order to estimate the error introduced by this
approximation, the vector impulse transfer function (Eq. 4.67)
was evaluated twice; first using Eq. 4.62 to predict Θ_2 and
then with Θ_2 given by the following equivalent approxima-
tion*

$$\Theta_2 = \pi + \Theta_1 + \rho_r + \rho_L$$
$$\text{or} \quad \Theta_2 = \pi \quad \text{if} \quad \pi - \Theta_1 + \rho_r + \rho_L > \pi \qquad 6.4$$

These two evaluations were used to calculate the percentage
errors H_I and H_Q, where H_I and H_Q are defined by

$$H_{I,Q} = \frac{G_{I,Q} - G'_{I,Q}}{G'_{I,Q}} \qquad\qquad 6.5$$

The subscripts I and Q refer to the first and second com-
ponents of the vector $\vec{G}(t,t')$ and the primed $\vec{G}$ refers to
results obtained using Eq. 6.4 rather than 4.62.

Percentage errors calculated from Eq. 6.5 are presented
for doubly scattered lidar returns from three different cloud

---

*In Eq. 4.62 η was set to its minimum possible value $\eta = 0$,
while in Eq. 6.4 η is set to its maximum possible value
where $\eta = \rho_r + \rho_L$.

models in Figs. 6.3, 6.4 and 6.5. These calculations assume
an angular distribution of transmitted energy given by

$$g(\rho) \propto \exp\left\{-\left(\rho / 5\times10^{-4}\,\text{rad.}\right)^2\right\}$$ 6.6

The following values for the half-angle transmitted beam
divergence ρ_L and the cloud base altitude x_c were assumed

$$\rho_L = 1 \text{ mr}$$
$$x_c = 1000 \text{ m.}$$ 6.7

The range of uncertainty in G_I and G_Q due to the θ_2-
approximation can be estimated from these figures. H_I and H_Q
are calculated with η set to its extreme values and are
therefore likely to overestimate the actual errors.

Notice that the H_Q values presented for cloud C-1 and
haze M are smaller than the estimated quadrature errors;
therefore the erractic behavior of these quantities is
probably due to integration errors.

Errors introduced by the θ_2-approximation have the
strongest effect in the calculation of the cross-polarized
doubly scattered return with Eq. 5.5. This determination
is particularly sensitive to these errors because it involves
a difference between the components G_I and G_Q. The examples
presented in Figs. 6.3, 6.4 and 6.5 indicate that the effect
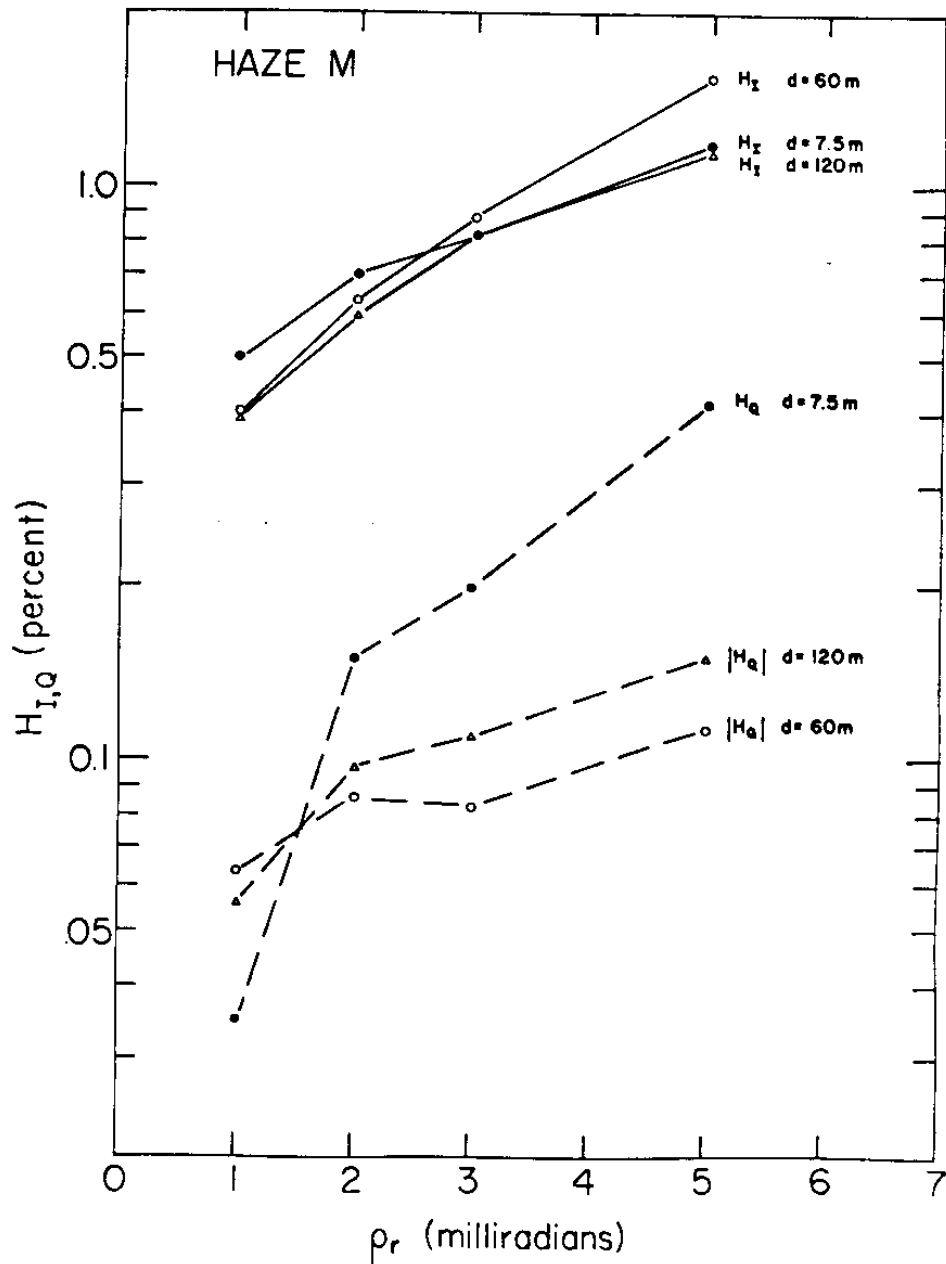is to overestimate the cross-polarized return.

Fig. 6.3 Estimates of an upper limit for the percentage errors H_I and H_Q (Eq. 6.5) induced in G_I and G_Q by the Θ_2-approximation. ρ_r is the receiver half angle field of view, the penetration depth d = c(t-t')/2 - x_c, evaluated for haze model M.
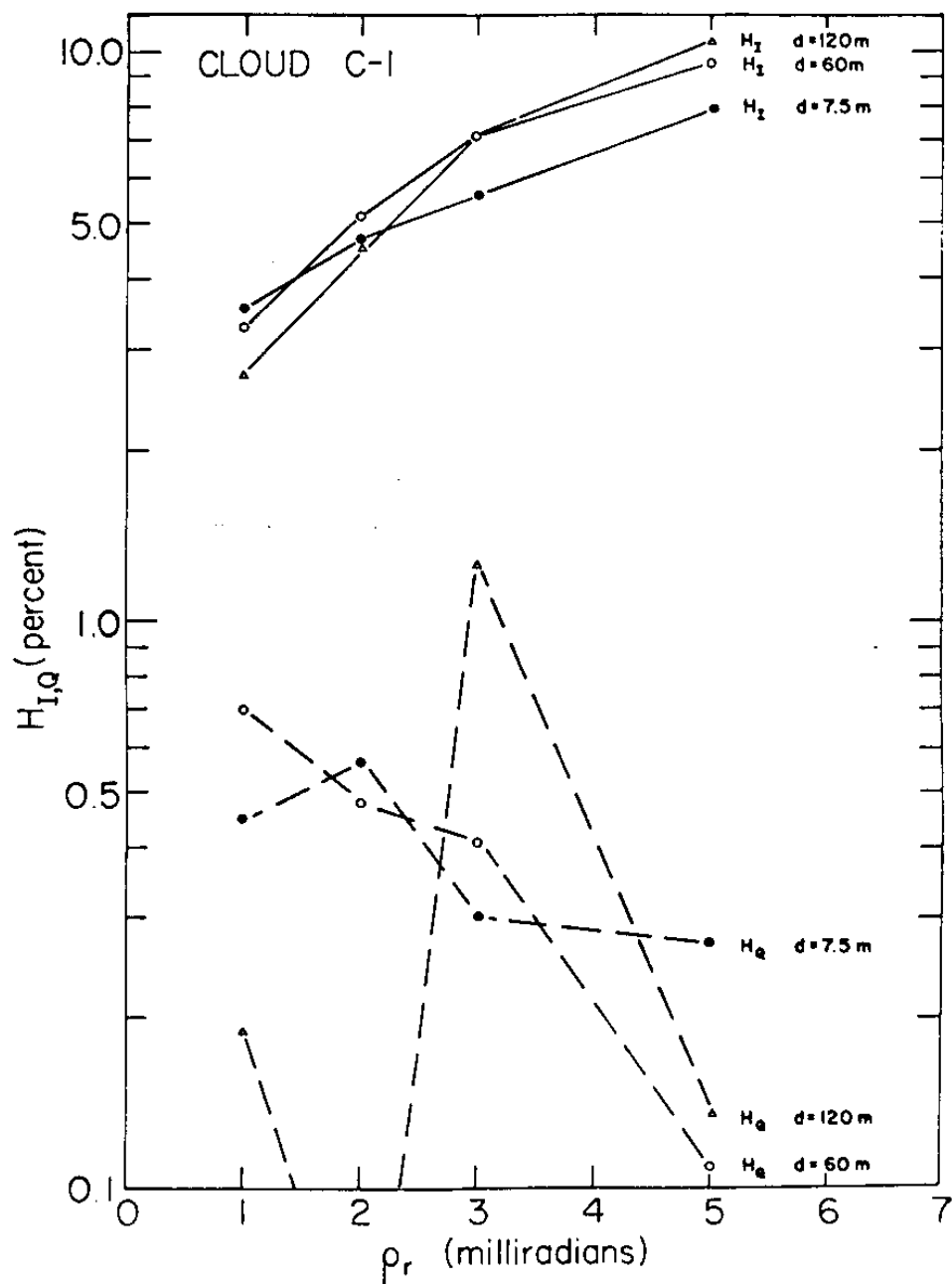
Fig. 6.4 Estimates of an upper limit for the percentage errors H_I and H_Q induced in G_I and G_Q by the θ_2-approximation. The particle size distribution is given by the cloud C-1 model.
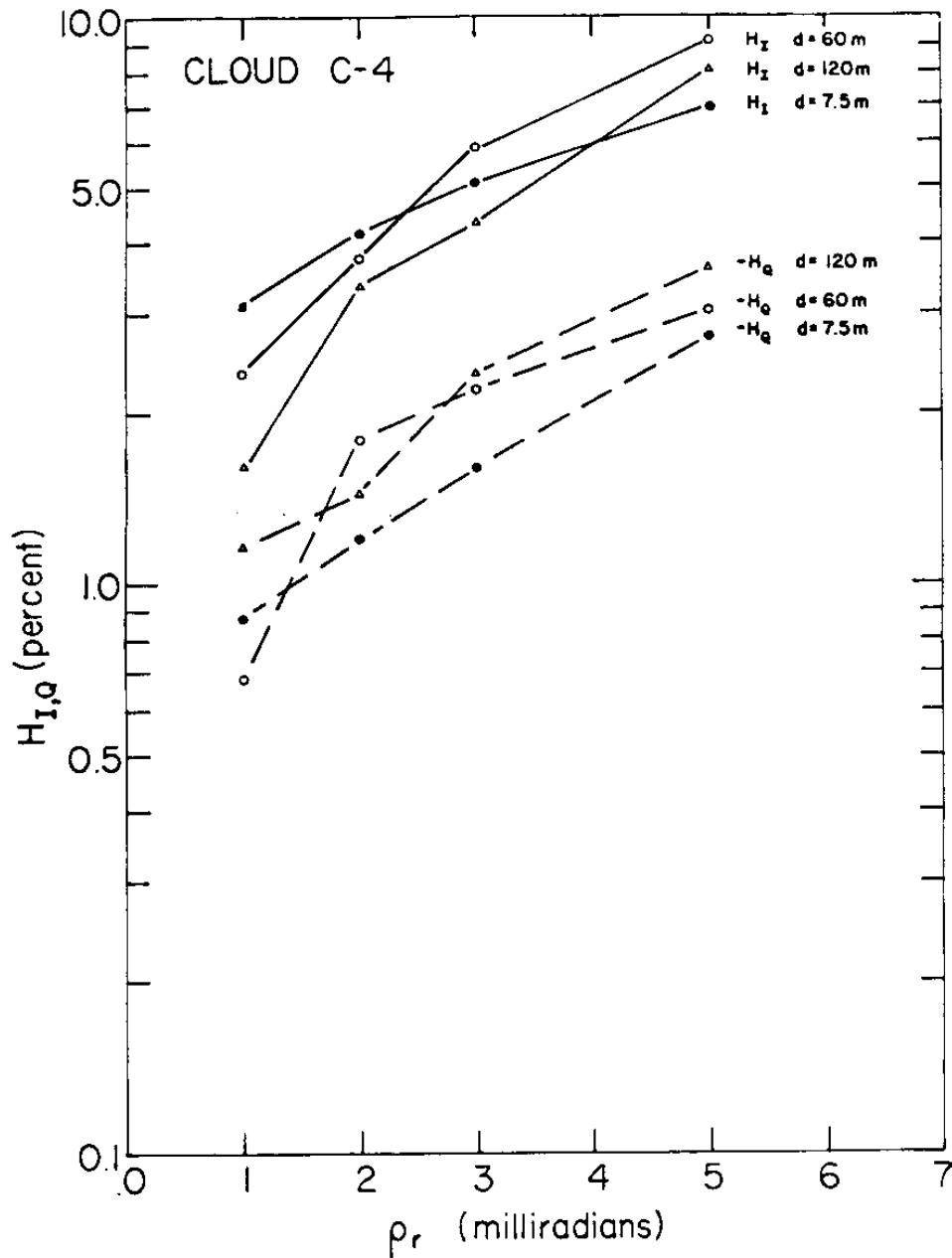
Fig. 6.5 Estimates of an upper limit for the percentage errors H_I and H_Q induced by the Θ_2-approximation. The particle size is given by the cloud C-4 model.

7. CALCULATED EXAMPLES OF $\vec{G}(t,t')$

In this section the numerical quadrature described in section 6.1 is applied to Eq. 4.67. This evaluation yields the Stokes vector impulse transfer function $\vec{G}(t,t')$. The dependence of $\vec{G}$ on three parameters will be considered: 1) the receiver angular field of view, 2) the particle size distribution in the cloud, 3) the cloud base altitude. The calculated values of $\vec{G}$ will also be compared to the approximate results of sections 3 and 5.

The double scattering calculations of this paper could be presented directly in terms of the doubly scattered power or the ratio of double to single scattering; however, these more intuitive quantities are less flexible in application and contain less information than the vector transfer function $G(t,t')$.

Only one evaluation of $\vec{G}$ is necessary for a given system geometry, cloud base altitude and particle size distribution. Then with the aid of Eq. 4.66, or one of its special case forms, the doubly scattered power can easily be obtained for any combination of transmitted energy, scattering cross section* and **receiver polarizing filter.**

For all examples presented in this section, the trans-

---

*Notice that for a fixed size distribution the scattering cross section is directly proportional to the number density of cloud droplets.

mitter is assumed to emit linearly polarized light, and all of the transmitted energy is assumed to be contained in a cone with an angular divergence $2\rho_L = 2$ milliradians. The radiation pattern is axially symmetric, but varies with the divergence angle ρ as follows

$$g(\rho) \propto \exp\left[-\left(\rho/5\times 10^{-4}\right)^2\right] \qquad 7.1$$

It is useful to compare the results obtained from Eq. 4.67 with the approximation presented in section 3. These comparisons require an expression corresponding to $\vec{G}$ for the approximate case. If the single scattering term of Eq. 3.8 is substituted into Eq. 3.10 and the order of the scattering N is taken equal to 2, an approximate double scattering equation results. A term by term comparison of this equation with 4.66 produces an expression which must represent G_I for the approximate solution:

$$G_I = \frac{1}{2} \frac{\langle P_1(\pi)\rangle_\lambda}{4\pi} \frac{d}{(x_c + d)^2} \qquad 7.2$$

where the penetration depth d is given by:

$$d = \frac{c(t-t')}{2} - x_c. \qquad 7.3$$

Notice that if a photon is transmitted at time t' and received at time t, then 2d is the distance the photon travels inside the cloud. The distance d can also be interpreted

as the penetration depth of a singly scattered phton.

The approximate solution presented in section 3 is valid only until photons scattered in the diffraction peak begin to escape from the receiver field of view. The penetration depth d_c at which approximation 7.2 is expected to break down can be obtained from the condition on the receiver field of view introduced in Eq. 3.16. This depth is

$$d_c = \frac{x_c(\rho_r - \rho_L)}{(N-1)\cdot\Theta_d} \qquad 7.4$$

where x_c = cloud base altitude

ρ_r = half-angle receiver field of view

N = order of scattering

Θ_d = angular width of the diffraction peak.

ρ_L = half-angle transmitted beam divergence

7.1 The angular field of view dependence

Unlike the case of the singly scattered lidar return where increasing the receiver acceptance angle beyond the transmitted beam divergence does not increase the received signal, the doubly scattered power continues to increase as the receiver acceptance angle is increased. The difference lies in how large a cloud volume is illuminated. In the double scattering case photons can be scattered out of the primary beam to illuminate the surrounding cloud, while

for single scattering only the directly illuminated volume can contribute to the observed return. This dependence is illustrated in Fig. 7.1 where the values of G(d) increase with penetration depth. A particle size distribution given by cloud model C-1 (see Appendix A) and a cloud base altitude of 1 km are assumed.

The approximate expression presented in Eq. 7.2 is also plotted in Fig. 7.1. According to Eq. 7.4 this approximation should be valid up to a penetration depth d_c, for the values of half-angle receiver field of view ρ_r considered in Fig. 7.1 the values of d_c are

ρ_r rad.	d_c	
1×10^{-3}	0	7.5
2×10^{-3}	29 m	
3×10^{-3}	57 m	
5×10^{-3}	115 m	

where $\theta_d = 33 \times 10^{-3}$ radians.

This value of θ_d is the r.m.s. angular width of the diffraction peak. It was calculated for cloud model C-1 with the approximation presented in Appendix A.

Notice that the approximate solutions based on he simple arguments presented in section 3 provide a good estimate of G_I throughout their predicted range of validity. This agreement provides evidence that, at least for the G_I component, the derivation of section 4 is without major error and that the computer evaluation of Eq. 4.67 is pro-
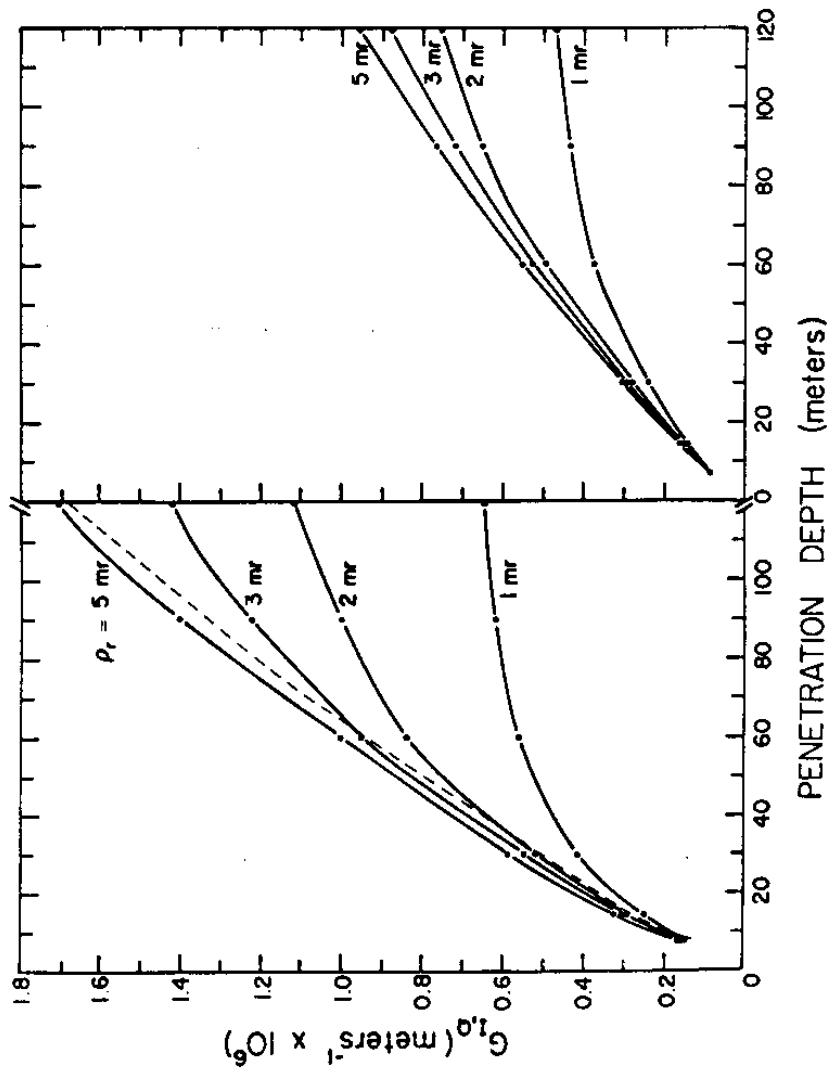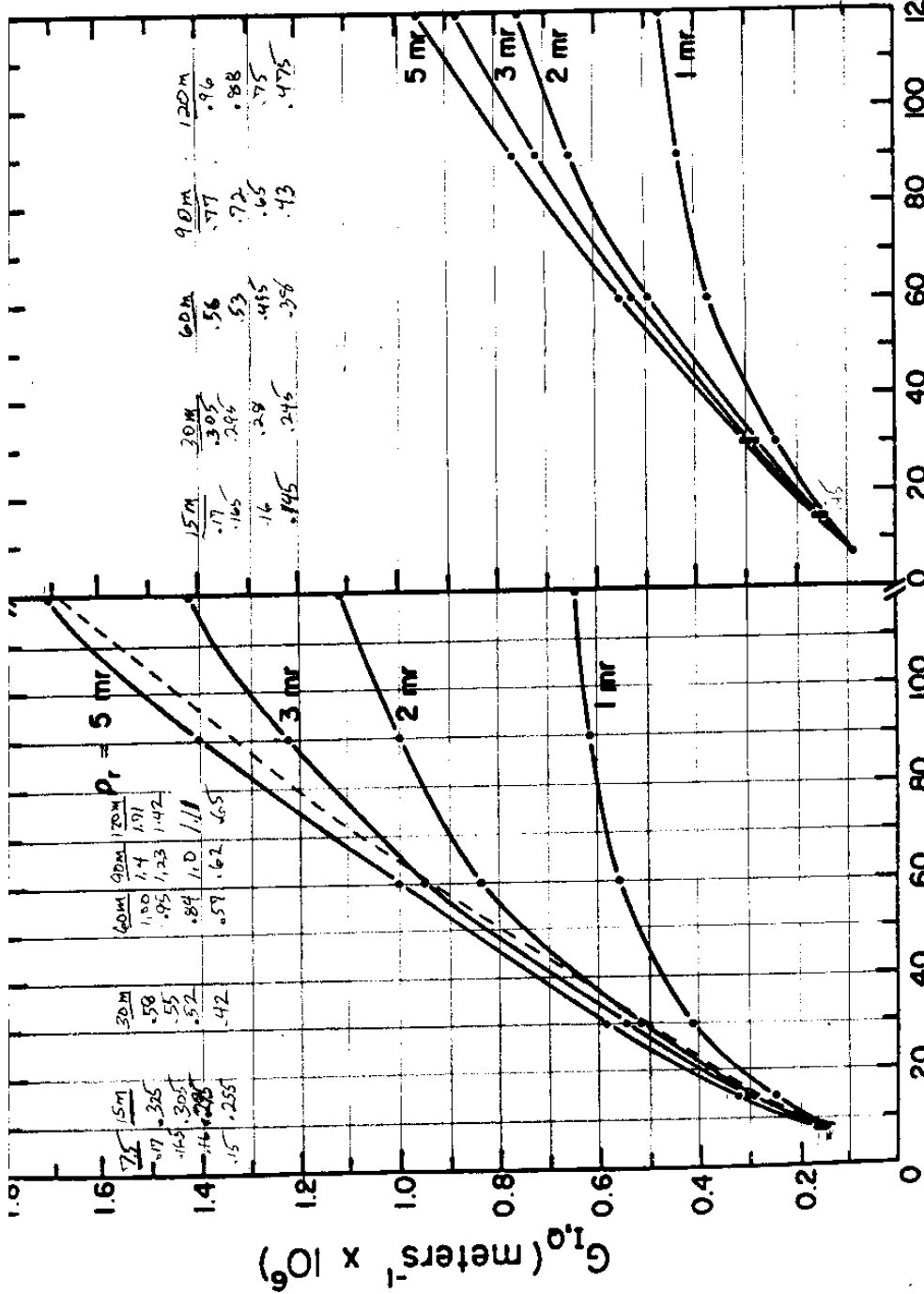
Fig. 7.1 Vector components (solid lines) G_r (left) and G_q (right) as a function of the penetration depth and the receiver half angle field of view, ρ_r. The approximation to G_T (Eq. 7.2) is the dashed line. Calculated for cloud model C-1 and a cloud base altitude $x_c = 1$ km.

on of
roxima-
a cloud

$$P_2 = E_0 \, A \, C \, \beta^2 \, C(t) \, e^{-2\beta d}$$

$$P_1 = E_0 \frac{C}{2} \frac{A}{r^2} \beta \frac{P(180)}{4\pi} e^{-2\beta d}$$

$$\frac{P_2}{P_1} = 2 r^2 \beta \frac{C(t)}{\frac{P(180)}{4\pi}} = 2 \left(r_c + d\right)^2 \beta \frac{C(t)}{\frac{P(180)}{4\pi}}$$

$$\beta = .0167$$

$$\frac{P(180)}{4\pi} = 0.05055$$

Half angle divergence = 2mm

d	C	P_2/P_1
7.5	0.16	0.1073
15.0	0.295	0.2008
30.0	0.52	0.3645
60.0	0.84	0.6234
90.0	1.0	0.785
120.0	1.15	0.92

ceeding correctly. In addition, this comparison indicates that the primary assumption used in the approximation must be valid, i.e. the dominant contribution to the doubly scattered return is produced by photons which are directed towards the receiver through a combination of a small angle diffraction peak scattering event and a large angle deflection which turns the photon back towards the receiver*. These scatterings may occur in any order with either the small or the large angle scattering happening first.

Eq. 7.2 is derived from Eq. 3.10, thus agreement of 7.2 with the "exact" values of G_I indicates that Eq. 3.10 is likely to provide reasonable estimates of third and higher order scattering as well. Of course the range of validity of these approximations must decrease rapidly with scattering order as predicted by Eq. 7.4.

In section 5.4 a special case solution, which assumed a small transmitted beam divergence and a Gaussian diffraction peak, was derived for G_I. In Fig. 7.2 this solution is compared to the values of G_I obtained by numerical integration of Eq. 4.67. The quadrature solutions presented in Fig. 7.2 are identical to those of Fig. 7.1 except that, in this figure, they are presented for a larger range of penetration depths. The special case solutions are derived using values of $\dfrac{\langle P_{(\pi)} \rangle}{4\pi}$ and $\sqrt{\langle \theta^2 \rangle}$ derived from Eq. 3.11 and

*This conclusion has also been verified by examining the relative contribution made by various angular segments to the θ_I-integral of Eq. 4.67.
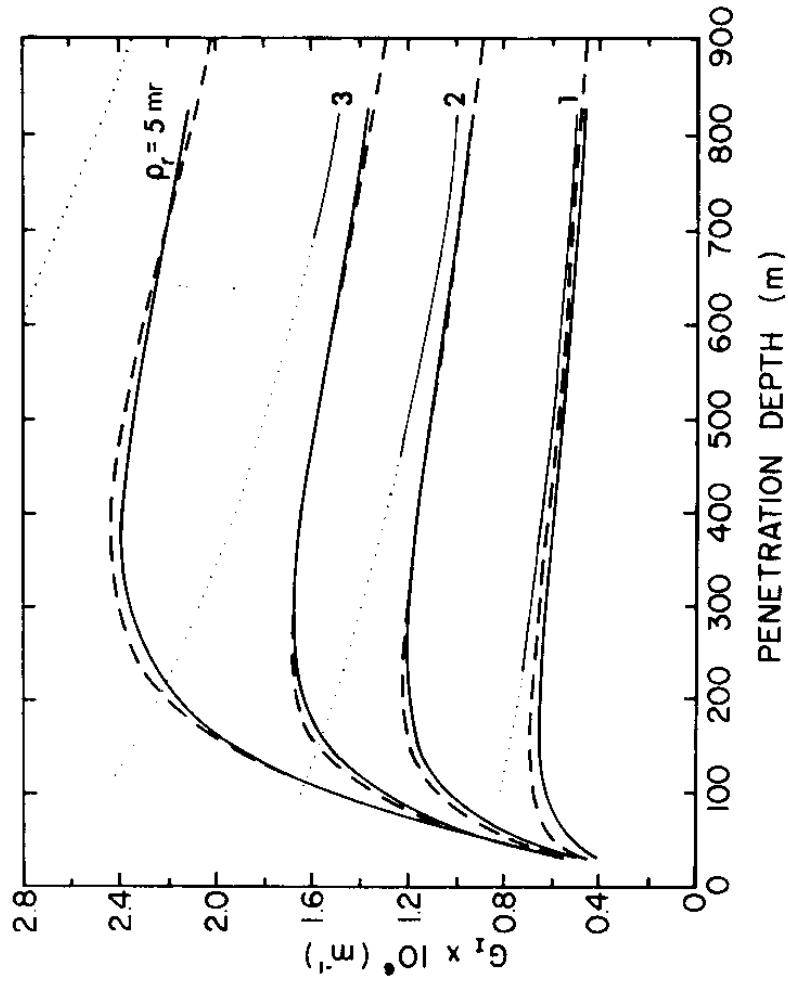
Fig. 7.2 Comparison between G_I values obtained by numerical integration of Eq. 4.67 (heavy solid lines) and special case solutions for Gaussian diffraction peak (Eq. 5.11, dashed lines) and Gaussian diffraction peak at large penetration depths (Eq. 5.14, dotted lines changing to light solid in range of validity (Eq. 7.7)).

77

Appendix A respectively. For cloud model C-1 these values are

$$\frac{\langle P_1(\pi) \rangle_{1/2}}{4\pi} = 0.035$$

$$\sqrt{\langle \theta^2 \rangle} = 0.034. \tag{7.6}$$

The close agreement observed between the special case solution for G_I and the values obtained directly for Eq. 4.67 illustrates the value of Eq. 5.11 in estimating the doubly scattered contribution to a lidar return.

Also plotted in Fig. 7.2 is the deep penetration approximation to G_I presented in Eq. 5.14. According to the discussion of section 5.4 this equation should be valid for the case $\rho_r << \sqrt{\langle \theta^2 \rangle}$ and for penetration depths greater than d_m, where

$$d_m = \frac{x_c \cdot \rho_r}{\left(0.18 \sqrt{\langle \theta^2 \rangle} - \rho_L \right)} \tag{7.7}$$

Notice that, as expected, the approximation improves as the $\rho_r / \sqrt{\langle \theta^2 \rangle}$ ratio decreases.

7.2 Size distribution dependence

Fig. 7.3 presents the vector components G_I and G_q for the C-1, C-3, C-4 and haze M particle size distributions introduced in Appendix A. Approximate values of G_I calculated for the special case solution for a Gaussian diffrac-
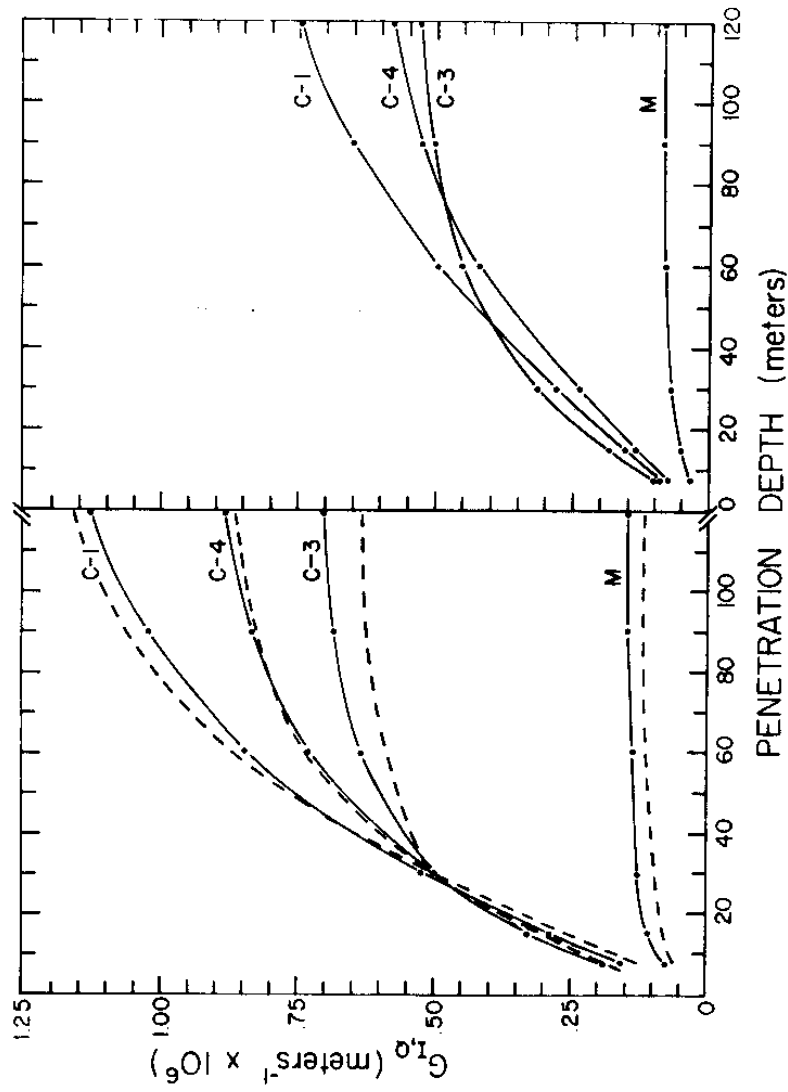
Fig. 7.3 Vector components (solid lines) G_I (left) and G_Q (right) as a function of penetration depth for several size distribution models. G_I values based on the Gaussian diffraction peak approximation (Eq. 5.11) are plotted as dashed lines.

tion peak (Eq. 5.11) are also plotted in this figure. A cloud base altitude of 1 km and a receiver field of view $2\rho_r = 4 \times 10^{-3}$ radians are assumed for all calculations presented here.

The Gaussian diffraction peak approximation to G_I (Eq. 5.11) is a function of the ratio $\rho_r/\sqrt{\langle\theta^2\rangle}$. Except for the scaling of the entire double scatter profile by the $\frac{\langle P_1(\pi)\rangle_2}{4\pi}$ term, this expression is otherwise independent of particle size dependent parameters. Changes in the particle size distribution which affect the width of the diffraction peak can therefore be expected to affect the shape of the $G_I(d)$ curve in a manner similar to changes in the receiver field of view. This diffraction peak width effect is clearly evident in Fig. 7.3. The wider the diffraction peak the sooner the $G_I(d)$ curve flattens out. This flattening occurs because some of the photons scattered into the diffraction peak propagate out of the receiver field of view before they undergo a second scattering. Either widening the receiver field of view or narrowing the diffraction peak, therefore, effects a similar reduction in this loss of photons.

The strong dependence of G_I on the ratio $\rho_r/\sqrt{\langle\theta^2\rangle}$ opens the possibility of remotely determining $\sqrt{\langle\theta^2\rangle}$ with lidar measurements of double scattering. Because the r.m.s. diffraction peak scattering angle $\sqrt{\langle\theta^2\rangle}$ is strongly dependent on particle sizes, such measurements could yield information on the scattering particles. Before such particle

size information can be acquired from lidar measurements,
however, it is likely that the present theory will require
extension to include the effects of higher order scattering
and spatial inhomogeneities in the clouds.

7.3 Cloud base altitude dependence

Fig. 7.4 presents the components of $\vec{G}$ for several
values of the cloud base altitude. A water droplet size
distribution given by model C-1 was assumed along with a
receiver acceptance angle given by $2\rho_r = 4$ mr. The simple
approximation developed in section 3 is also plotted in
this figure. Once again, in its range of applicability
the small penetration depth approximation (Eq. 7.2) provides
a good fit to the results obtained by numerical integration
of Eq. 4.67. The values of the maximum penetration depth d_c
for which the approximation is valid can be obtained from
Eq. 7.4. These values are

d_c(meters)	x_c(meters)
16	500
33	1000
49	1500
66	2000

7.8

The lower the cloud base altitude the more quickly the
exact calculations depart from the approximate solutions.
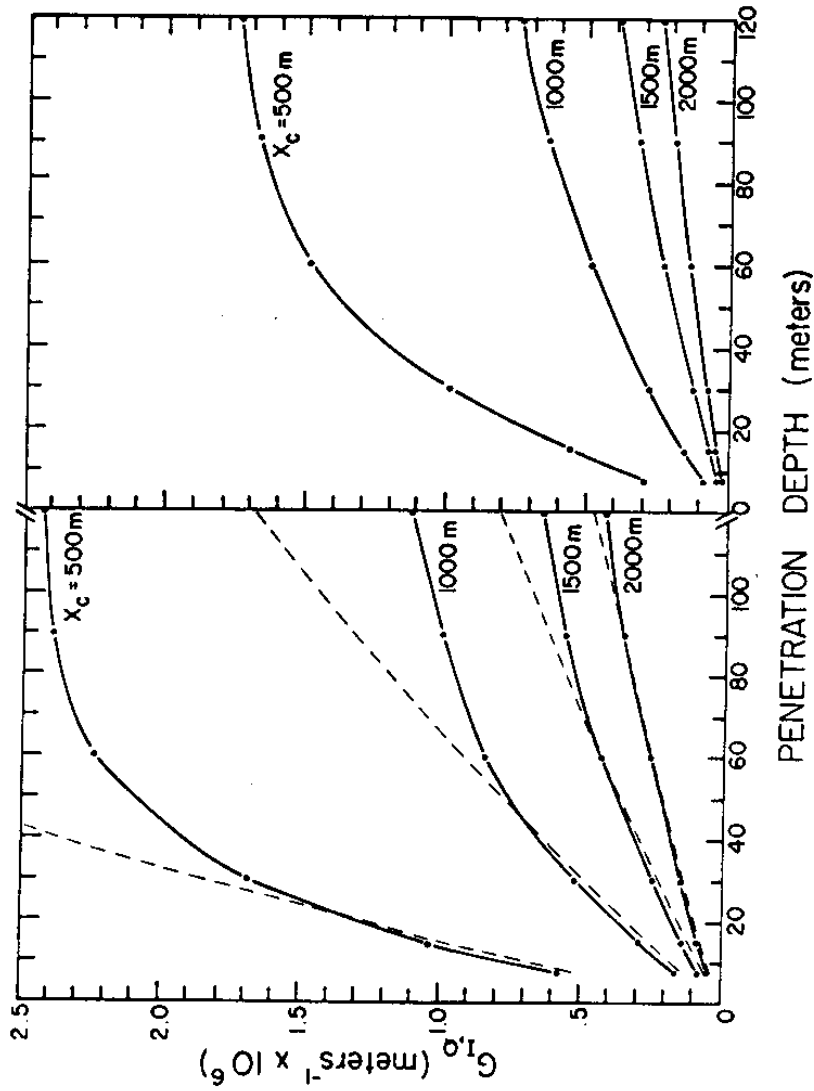For a given ρ_r the diameter of the receiver acceptance cone

Fig. 7.4 Vector components (solid) G_I (left) and G_Q (right) as functions of penetration depth and cloud base altitude, x_c. Approximate values of G_I (Eq. 7.2) are presented as dashed lines. These calculations assume: cloud model C-1, receiver half angle field of view ($\rho_r = 0.002$ r, and a laser half angle divergence ($\rho_L = 0.001$r.

increases with altitude; therefore, at low altitudes a photon deflected by a small angle propagates out of the receiver field of view more quickly.

The special case solution for a Gaussian diffraction peak, although not plotted here, also yields a good fit to the values presented in Fig. 7.4.

8. COMPARISONS WITH PREVIOUS CALCULATIONS

8.1 Liou and Schotland

In section 3 calculations of the doubly scattered
return performed by Liou and Schotland (1971) were compared
to an approximate solution. This comparison showed a dis-
crepancy between their exact solution and the approximation.
In order to investigate this further Eq. 5.5 was used to
derive the expected doubly scattered lidar return for the
system geometry and cloud model used by Liou and Schotland.
These values were then divided by the expected singly scat-
tered return to produce the same double to single scatter
ratios published by L & S. These results are presented in
Fig. 8.1. Cloud model C-1 is assumed for these calculations[*];
the other system and cloud parameters used are:

$$x_c = 1000 \text{ m}$$
$$\beta_s = 0.0168 \text{ m}^{-1}$$
$$\rho_r = 5 \times 10^{-3} \text{ r}$$
$$\rho_L = 5 \times 10^{-3} \text{ r}$$
$$g(\rho) \propto e^{-(\rho/4\times10^{-3})^2}$$

8.1

---

[*]Cloud model C-1 in the notation used in this development
is identical to cloud model C-4 in the identification scheme
used by Liou and Schotland. The cloud models used in the
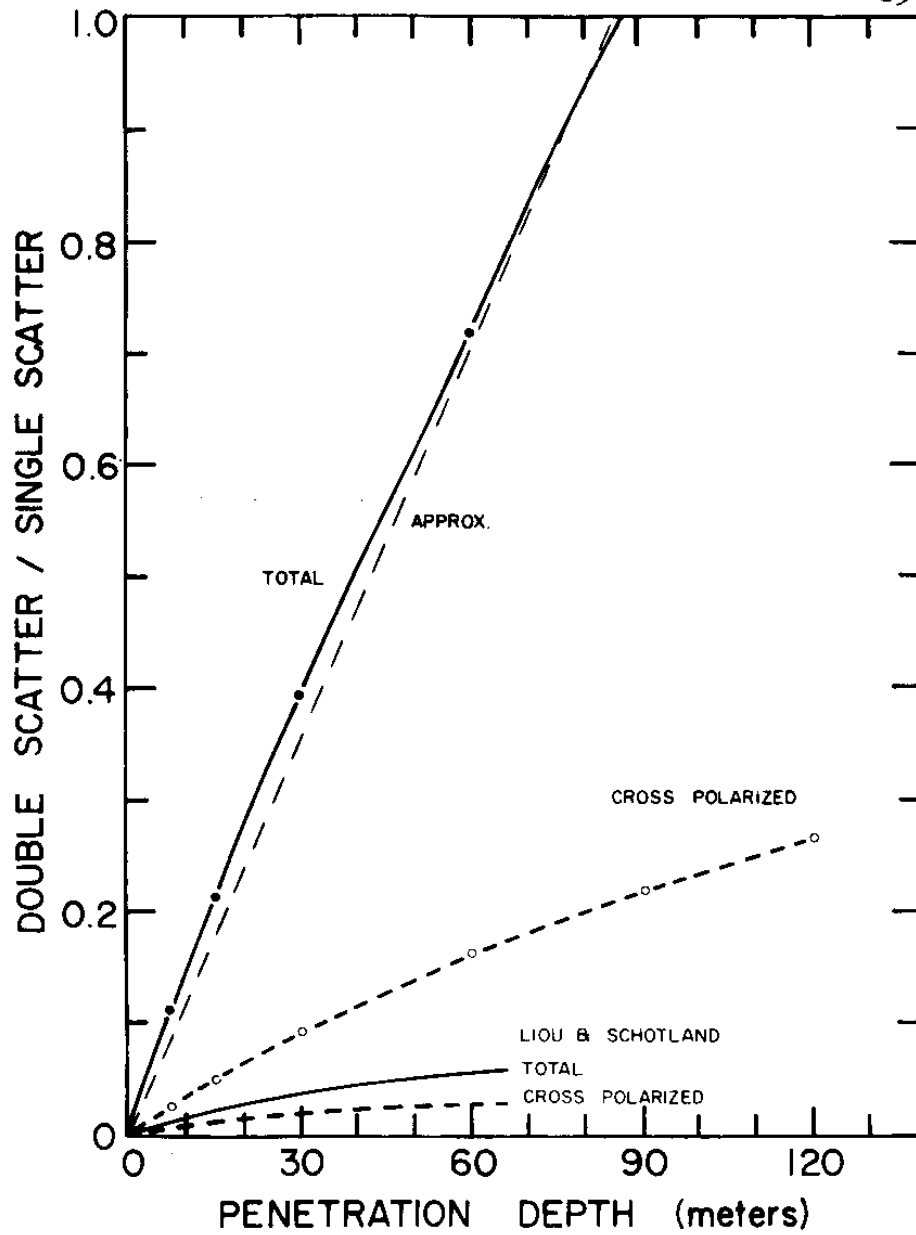present development correspond to those introduced by
Deirmendjian (1969).

Fig. 8.1 A comparison between the double to single scatter ratios obtained in the present analysis and those obtained by Liou and Schotland (1971). Curves with data points are the present results. The small penetration depth approximation (Eq. 3.10) is also shown.

The approximate solution developed in section 3 is also plotted in Fig. 8.1. For the penetration depths considered here the total double scattering calculated from Eq. 5.5 and the approximate solution show excellent agreement; however, the total double scatter calculated by Liou and Schotland for the same cloud model and system geometry is more than a factor of ten smaller. The computed cross polarized scattered returns also exhibit substantial disagreement. Liou and Schotland's results are more than a factor of five smaller than the values calculated from Eq. 5.5.

Liou and Schotland also calculate a depolarization ratio Δ which is defined as follows:

$$\Delta = \frac{\theta_{2,\perp}}{\theta_1 + \theta_{2,\parallel}} \qquad 8.2$$

where $\theta_{2,\perp}$ = doubly scattered power with polarization perpendicular to the transmitted polarization

$\theta_{2,\parallel}$ = doubly scattered power with polarization parallel to the transmitted polarization

θ_1 = singly scattered power.

The double to single scatter ratios presented in Fig. 8.1 were used to derive values of the depolarization ratio. A comparison of these results and the values published by Liou and Schotland are contained in Fig. 8.2. The depolarization ratios based on the present double scatter analysis
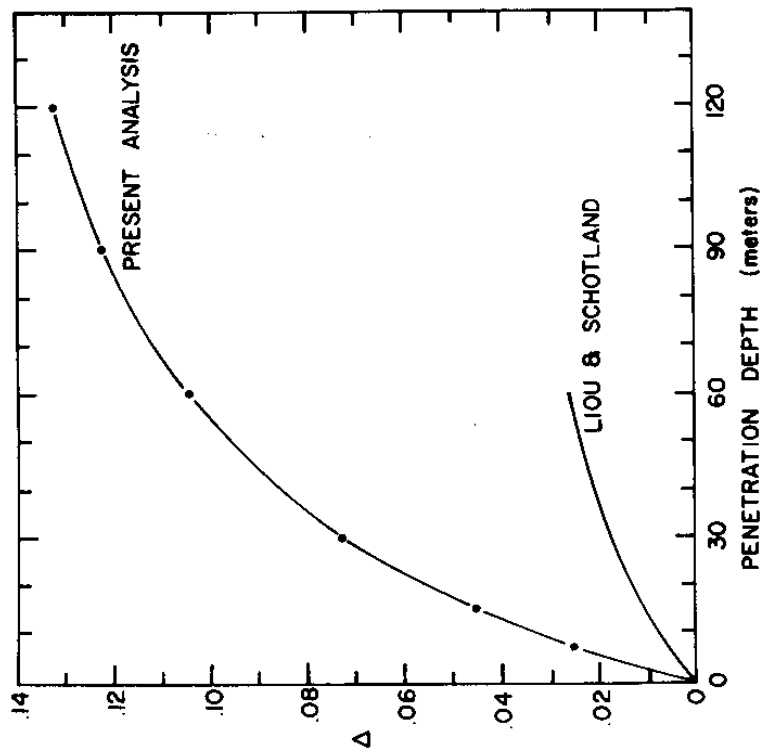
Fig. 8.2 The depolarization ratio Δ (Eq. 8.2) as a function of penetration depth. Results of the present analysis are compared to those of Liou and Schotland (1971).

are about four times as large as the Liou and Schotland results. Furthermore, since the approximate solutions developed in section 3 indicate that third and higher order scattering is not negligible, actual measurements should contain additional depolarization due to higher order scattering.

8.2 Plass and Kattawar

In this section doubly scattered returns calculated from Eq. 5.3 are compared to the results obtained by Plass and Kattawar with a Monte Carlo procedure. This comparison is restricted to a single case involving a rather unrealistic cloud comprised of particles with a haze C size distribution. Computation of the doubly scattered return for the more realistic nimbostratus model presented by Plass and Kattawar would have involved the time consuming computer computation of Mie scattering intensities to derive the scattering matrix for this size distribution.

Fig. 8.3 presents a comparison of the multiply scattered return calculated by Plass and Kattawar and the double scattering derived from Eq. 5.3, both solutions assume a haze C particle size distribution. The other cloud and system parameters used are:
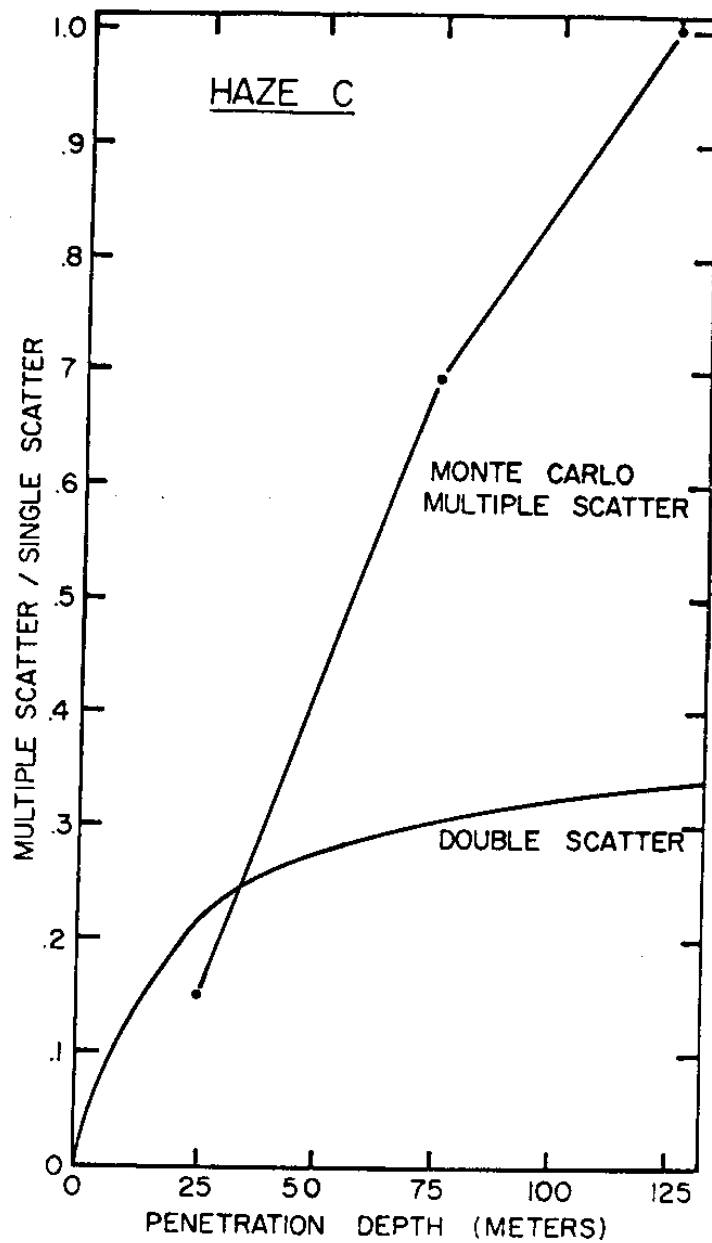
Fig. 8.3 The ratio of all multiple scattering to single
scattering derived with a Monte Carlo simulation by Plass
and Kattawar (1971) and the ratio of double to single scat-
tering derived from the present analysis for the same sys-
tem and cloud parameters.

$$x_c = 1000 \text{ m}$$

$$\beta_s = 0.01 \text{ m}^{-1}$$

$$\rho_r = 0.005 \text{ r}$$

$$\rho_L = 0.001 \text{ r}$$

8.3

$g(\rho)$ is independent of ρ.

The Monte Carlo computations include all orders of scattering, therefore, if both computations are correct, the difference between the Monte Carlo results and the double scatter values should represent the contribution due to third and higher order scattering. If this difference is taken for the values presented in Fig. 8.3, unreasonable results are obtained for penetration depths less than 35 m. In this region the double scatter calculations yield larger returns than those computed for all orders of scattering. This author believes that the discrepancy results from statistical errors in the Monte Carlo determination of multiple scattering. An examination of data points presented by Plass and Kattawar (1971) indicates scatter about a smooth curve which could, at a penetration depth of 25 m, easily result in as much as a factor of two error in the multiple to single scatter ratio. The multiply scattered return is derived by subtracting the singly scattered contribution from the total return; therefore, the error is greatest where the difference is small. It does not appear that the large difference between the double scatter and the total

scatter which appears beyond penetration depths of 50 m can result from statistical errors; this difference may therefore represent third and higher order scattering.

9. SUMMARY

Section 2 shows what appears to be a substantial dis-
crepancy between the multiply scattered lidar returns calcu-
lated by Liou and Schotland (1971) and those calculated by
Plass and Kattawar (1971).

Section 3 develops a small angle approximation for the
N$^\text{th}$ order contribution to a lidar return from a cloud. This
approximation is valid for small penetration depths into a
cloud consisting of particles which scatter light strongly
into a narrow diffraction peak. Within its range of appli-
cability this approximation yields multiply scattered re-
turns which appear consistant with results published by
Plass and Kattawar, but which are in clear disagreement with
values presented by Liou and Schotland.

In section 4 a Stokes vector impulse transfer function
is derived for double scattering. This transfer function
can be used to calculate the magnitude and polarization
of the doubly scattered lidar return from a homogeneous
cloud of spherical particles. The effects due to cloud base
altitude, finite angular spread of the transmitted pulse,
non-uniform distribution of the transmitted energy with
time and angle in the transmitted pulse, finite receiver
field of view, particle size distribution in the cloud and a
polarizing filter on the receiver are included in this deri-
vation.

In section 5 the vector transfer function for double
scattering developed in the previous section is presented
in simplified form for a number of special cases. These
cases include: 1) lidar system transmitting short pulses
(Eq. 5.1), 2) systems with an unpolarized receiver (Eq. 5.3),
3) systems using a linearly polarized receiver (Eq. 5.5),
4) systems with a small transmitted beam divergence (Eq. 5.7),
5) the case of a transmitter with small beam divergence
illuminating a cloud with a Gaussian angular dependence of
the forward scattering peak (Eq. 5.11), and 6) the same case
as 5 except that the system is immersed in the cloud and the
receiver field of view is small compared to the r.m.s. width
of the forward scattering peak (Eq. 5.14 and 5.15). Equation
5.11 is the most important result of this section. When-
ever the forward scattering peak can be approximated by a
Gaussian, the doubly scattered return can be obtained with-
out recourse to cumbersome numerical integrations.

Section 6 considers the details of obtaining values
for the transfer function derived in section 4. The
numerical integration scheme utilized is described and the
errors implicit in its use are investigated. The error intro-
duced by an approximation to the second scattering angle
made in section 4 is also investigated. The magnitudes
of these errors depend on both the system geometry and the
particle size distribution. In the worst case discussed,

cloud model C-1 and and 5 mr half-angle receiver field of
view, an upper limit for the combined errors is approxi-
mately 15% of the calculated return. This is a very con-
servative estimate and even in this worst case the actual
error is likely to be less than 7%.

In section 7 examples of the Stokes vector impulse
transfer function are presented. These results, which are
calculated from the equations derived in section 4, are
obtained for several size distributions, cloud base alti-
tudes and values of the receiver angular field of view.
These values of the vector impulse transfer function are
compared to an approximate equation based on the small angle
multiple scatter relationship developed in section 3. With-
in the range of penetration depths where the assumptions
used in the approximation are valid the approximate values
are in good agreement with the with the exact calculations.
This agreement along with an examination of partial results
during numerical integration of the equation for the vector
impulse transfer function indicates that the doubly scat-
tered lidar return from a cloud is dominated by photons
returned to the receiver through a combination of a small
angle deflection in the diffraction peak and a large angle
scattering near π radians. Significant returns are pro-
duced by both the scattering combination where the small
angle event occurs before the large angle event and by the

reverse combination. Results based on Eq. 5.11, the special case solution for a Gaussian diffraction peak, are compared to values obtained through numerical quadrature. This comparison shows good agreement between Eq. 5.11 and the exact solutions.

In section 8 the present doubly scattered lidar return calculations are compared to the results published by Liou and Schotland (1971) and Plass and Kattawar (1971). The total doubly scattered power resulting from the present analysis was found to be more than a factor of ten larger than values presented by Liou and Schotland; the cross polarized doubly scattered return was approximately a factor of four larger than their values. When these results were combined with the singly scattered return to calculate the ratio of the cross polarized return to the return with polarization parallel to the transmitted polarization, this ratio was also approximately a factor of four larger than that derived by Liou and Schotland.

Plass and Kattawar do not separate the second order scattering from the other orders of multiple scattering; it is therefore necessary to compare the present results to their determination of all multiple scattering. At very

small penetration depths the present doubly scattered re-
turns were shown to be larger than the Flass and Kattawar
estimate of total multiple scattering. This discrepancy,
however, appears to be within the statistical error bounds
of the Monte Carlo determination. At larger penetration
depths the Monte Carlo results are considerably larger than
the double scatter results; this is consistent with the
results of section 3 where it was concluded that third and
higher order scattering produced significant contributions
to the total lidar return received from a cloud.

10. CONCLUSIONS

The most important conclusion of this study is that lidar returns from terrestrial water clouds are likely to contain substantial contributions due to multiple scattering. For the most frequently used lidar system geometries and most cloud compositions the single scatter lidar equation is not adequate to describe the return signals.

The doubly scattered lidar return is strongly dependent on the ratio of the receiver acceptance angle to the angular width of the forward scattering peak caused by light diffracted around the cloud droplets. The return increases as this ratio is increased until all of the diffracted light is contained in the receiver field of view. Further increases produce relatively small changes in the doubly scattered return. When the diffraction peak is within the receiver field of view the doubly scattered signal becomes comparable to the singly scattered return at an optical thickness equal to one.

A simple physical model (Eq. 3.10) which estimates the doubly scattered return at small penetration depths, indicates that third and higher order contributions to a lidar return from a cloud may also be significant. This conclusion is supported by subtracting the present doubly scattered estimates from the Monte Carlo determination of all multiple scattering made by Plass and Kattawar

(1971); this difference is not zero, thus indicating the presence of higher order scattering.

The doubly scattered return is partially depolarized; for the cloud models considered in this study 20 to 30 percent of the doubly scattered signal was polarized in a direction perpendicular to the transmitted polarization. This depolarization along with the depolarization expected due to third and higher order scattering exists even though the scattering particles are perfectly spherical. Thus if lidar measurements are used to infer the presence of ice in a cloud through the depolarization of the singly scattered return caused by non-spherical crystals it will be necessary to distinguish between the depolarization due to particle asymmetries and depolarization due to multiple scattering.

Because the doubly scattered lidar return is strongly dependent on the ratio of receiver acceptance angle to the angular width of the scattering diffraction peak, it may be possible to determine the width of the diffraction peak remotely with lidar measurements. The diffraction peak is sensitive to particle size; thus, if the effects of cloud inhomogeneities and higher order scattering can be properly computed, double scatter measurements may allow remote determination of particle size information.

APPENDIX A. MODEL SCATTERING MATRICES

In problems concerning the scattering of polarized
light it is convenient to represent the intensity and polar-
ization of the light by means of a Stokes vector*. This
four component vector provides a complete description of an
incoherent beam of light. When an arbitrarily polarized
elecromagnetic wave is scattered by particles, both the in-
coming and the outgoing wave can be represented in Stokes
vector form. The transformation of the Stokes vector by
the scattering can be represented in terms of a 4 x 4 matrix
known as the Mueller matrix. The elements of this matrix
are functions of wavelength, size of the scattering particles,
complex index of refraction of the particles and shape of the
particles. Fortunately the small droplets which compose
terrestrial water clouds are both spherical and homogeneous;
for this special case the elements of the Mueller matrix
can be derived with the electromagnetic scattering theory
developed by Mie.

The multiple scattering calculations presented in this
paper use the scattering matrix elements derived from Mie

---

*A discussion of the Stokes vector representation of light
may be found in Shurcliff (1962). The application of the
Stokes vector and the associated Mueller matrix to electro-
magnetic scattering problems is discussed by a number of
authors including Chandrasekhar (1960), Deirmendjian (1969),
Kerker (1969), Perrin (1942) and van de Hulst (1957).

theory by Deirmendjian (1969). Because Deirmendjian employs a modified form of the Stokes vector, it was first necessary to transform his matrix elements for use with the present Stokes vector form.

The standard I,Q,U,V form of the Stokes vector can be obtained from the modified I_ℓ,I_r,U,V form with the following transformation

$$\begin{pmatrix} I \\ Q \\ U \\ V \end{pmatrix} = B \begin{pmatrix} I_\ell \\ I_r \\ U \\ V \end{pmatrix} \qquad\qquad A.1$$

where

$$B = \begin{pmatrix} 1 & 1 & 0 & 0 \\ 1 & -1 & 0 & 0 \\ 0 & 0 & 1 & 0 \\ 0 & 0 & 0 & 1 \end{pmatrix}.$$

Eq. A.1 can be used to show that any matrix M expressed in the I_ℓ,I_r,U,V system can be transformed to a matrix M' in the I,Q,U,V system with the simularity transform

$$M' = B M B^{-1} \qquad\qquad A.2$$

This transformation can be applied to the scattering matrix defined by Deirmendjian. If the elements of his matrix are represented by lower case "p," the scattering matrix "$\mathbb{P}$," with elements capital "P_i," used in the present study is given by

$$\mathbb{P}(\theta) = \begin{pmatrix} P_1 & P_2 & 0 & 0 \\ P_2 & P_1 & 0 & 0 \\ 0 & 0 & P_3 & P_4 \\ 0 & 0 & -P_4 & P_3 \end{pmatrix} = \begin{pmatrix} p_1+p_2 & p_1-p_2 & 0 & 0 \\ p_1-p_2 & p_1+p_2 & 0 & 0 \\ 0 & 0 & p_3 & p_4 \\ 0 & 0 & -p_4 & p_3 \end{pmatrix} \qquad A.3$$

Deirmendjian calculates the matrix elements for several particle size distributions and for a number of wavelengths of light. Because the ruby laser commonly used as a lidar transmitter emits at a wavelength of 0.6943 microns, Deirmendjians's 0.7 micron matrix elements are used exclusively in this paper.

The particle size distributions considered are of the modified gamma distribution type and are defined as follows

$$\eta(r) = a \cdot (r - \delta)^{\alpha} \cdot exp\left\{-b(r - \delta)^{\gamma}\right\}$$ A.4

The parameters $\alpha, \gamma, \delta, a$ and b used in Deirmendjian's calculations are given in Table A.1 and

$\qquad$ n(r) = number of particles per unit radius per

$\qquad\qquad$ unit volume

$\qquad$ r = particle radius (microns)

TABLE A.1

Size distribution parameters

Distribution type	a	α	γ	b	δ
Haze M	5.3333×10^{4}	1	½	8.9443	0
C-1	2.3730	6	1	3/2	0
C-3	5.5556	8	3	1/3	0
C-4	5.5556	8	3	1/3	2

In addition to the matrix elements for these distributions where the number of particles varies smoothly with size, the scattering matrix elements for the discontinuous haze C model are used. This size distribution which approximates the Junge type size distributions frequently observed in continental hazes is defined by

$$n(r) = 0 \qquad r \leq 0.03 \text{ microns}$$
$$n(r) = 1 \qquad 0.03 < r < 0.1 \text{ microns} \qquad \text{A.5}$$
$$n(r) = 10^{-4} r^{-4} \qquad 0.1 \leq r \quad \text{microns.}$$

The model particle size distributions presented above are illustrated in Fig. A.1. The plotted distributions are normalized such that, $n(r_c) = 1$ where r_c is the mode radius. This normalization is possible because the matrix elements are independent of the total number of scattering particles and depend only on the relative numbers in each size interval.

The cumulus cloud model C-1 has been shown (Liou and Schotland, 1971) to provide an approximate fit to the particle size distributions in fair weather cumulus clouds measured by Diem (1948) and Battan and Reitan (1957).

For the particle size distributions presented in Fig. A.1 Deirmendjian's phase matrix elements have been transformed to the I,Q,U,V form with Eq. A.3. The resulting matrix elements are illustrated in Figs. A.2, 3, 4, 5, and 6.

Notice that for the cloud models the matrix element P_1 shows a characteristic strong peaking for small angle
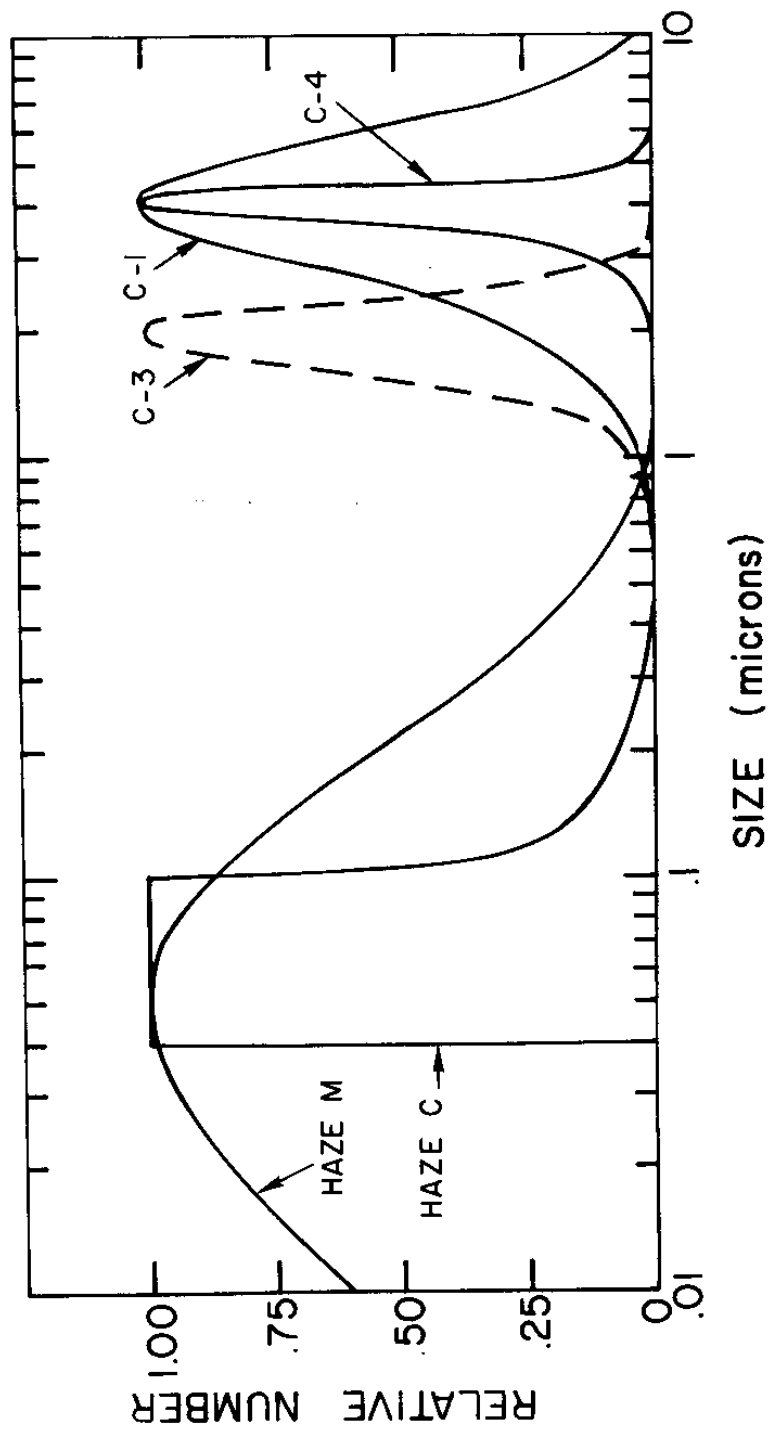
Fig. A.1 Paritcle size distribution expressed in terms of relative number of particles per micron.
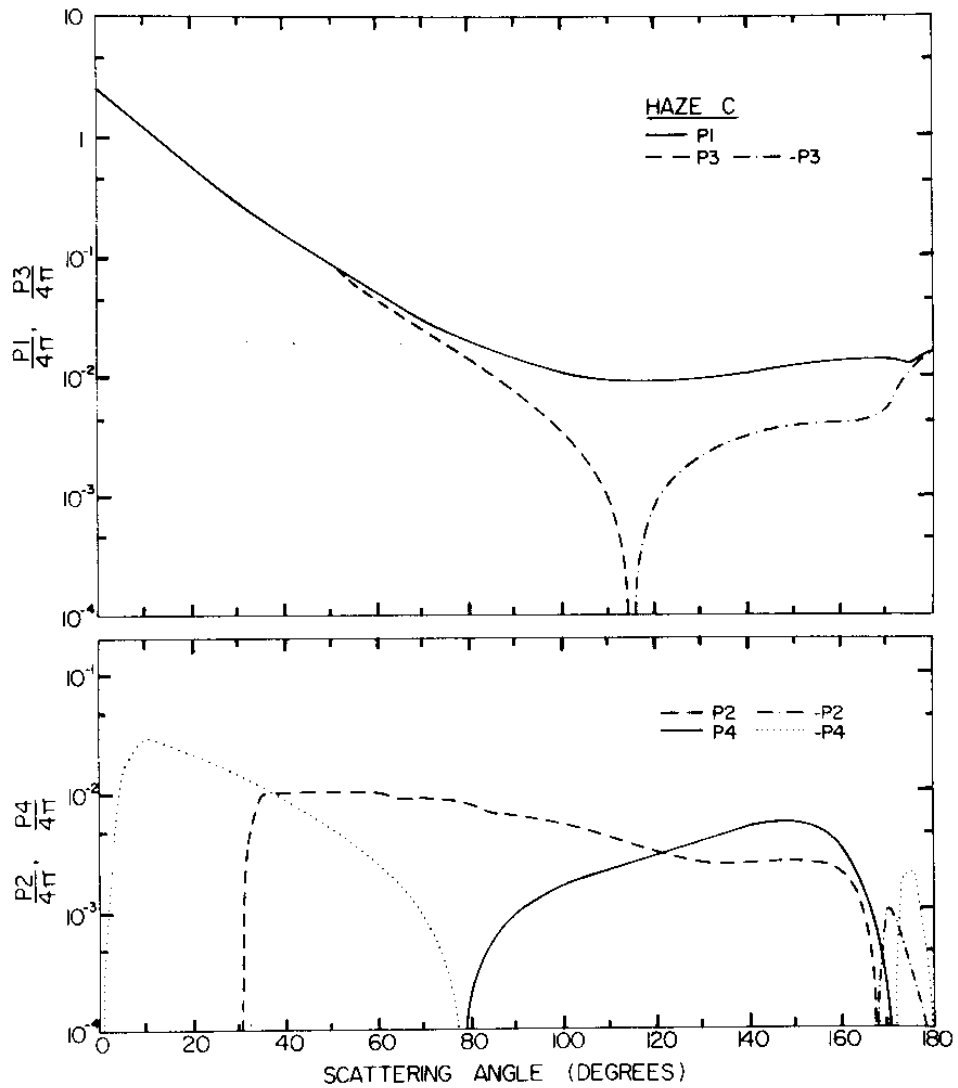
Fig. A.2 Scattering matrix elements for haze model 6.
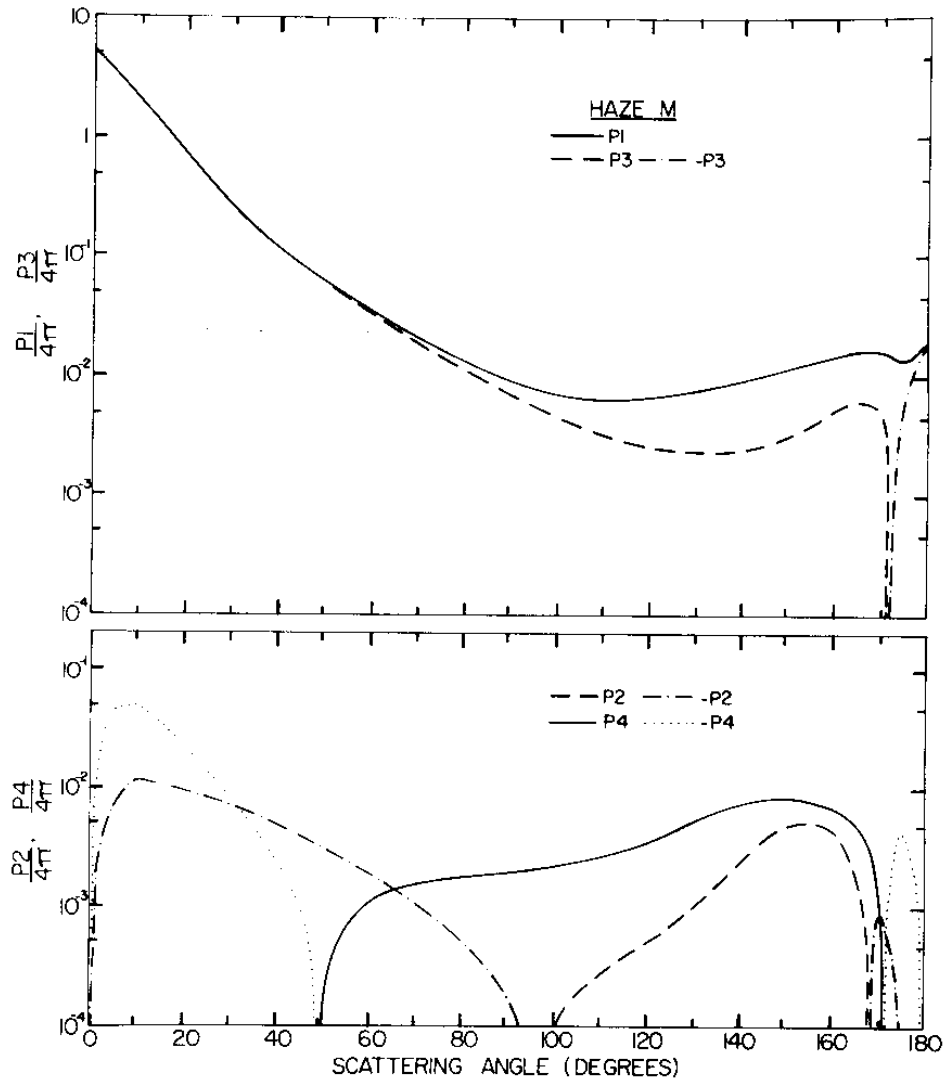Note that negative terms, indicated in key, are reflected
about the abscissa.

Fig. A.3 Scattering matrix elements for haze model M.
(Note that negative terms, indicated in key, are reflected
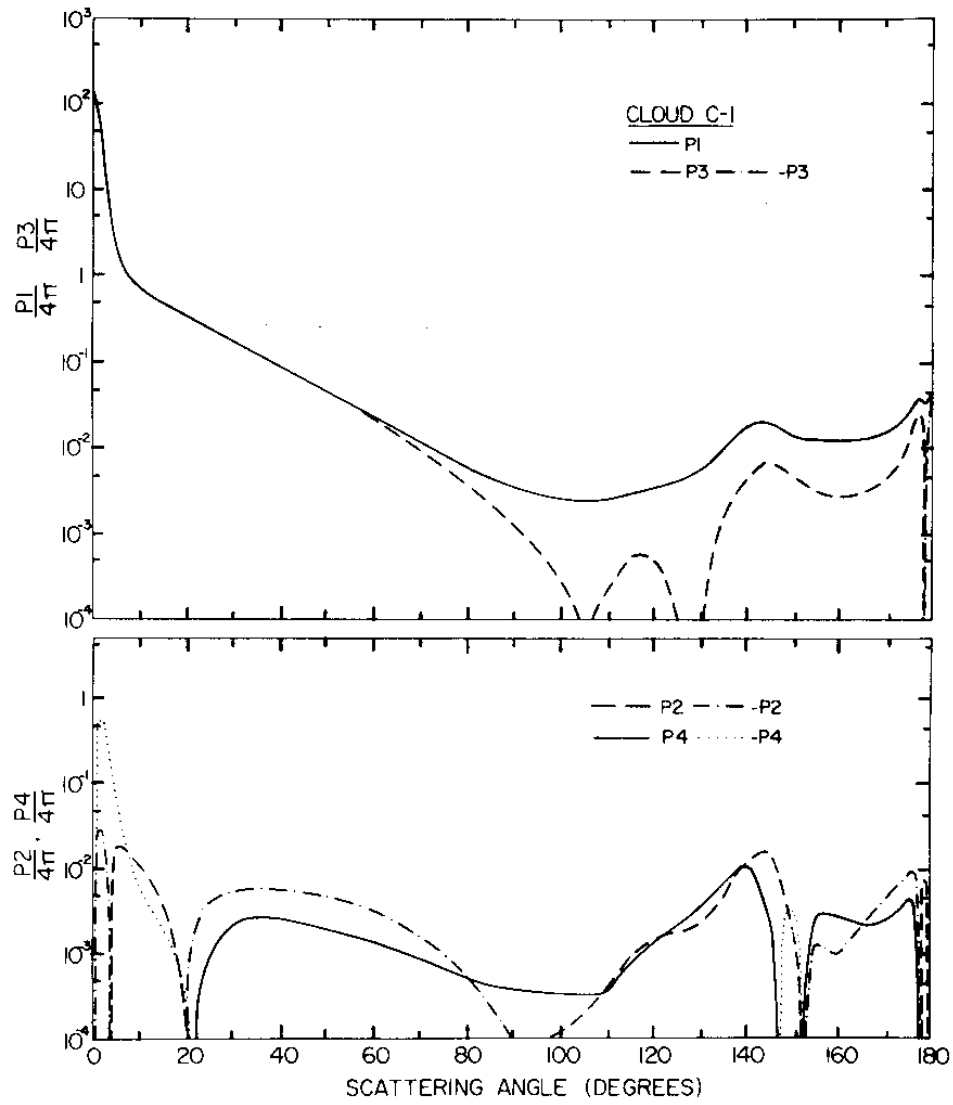about the abscissa.)

Fig. A.4   Scattering matrix elements for cloud model C-1.
(Note that negative terms, indicated in key, are reflected
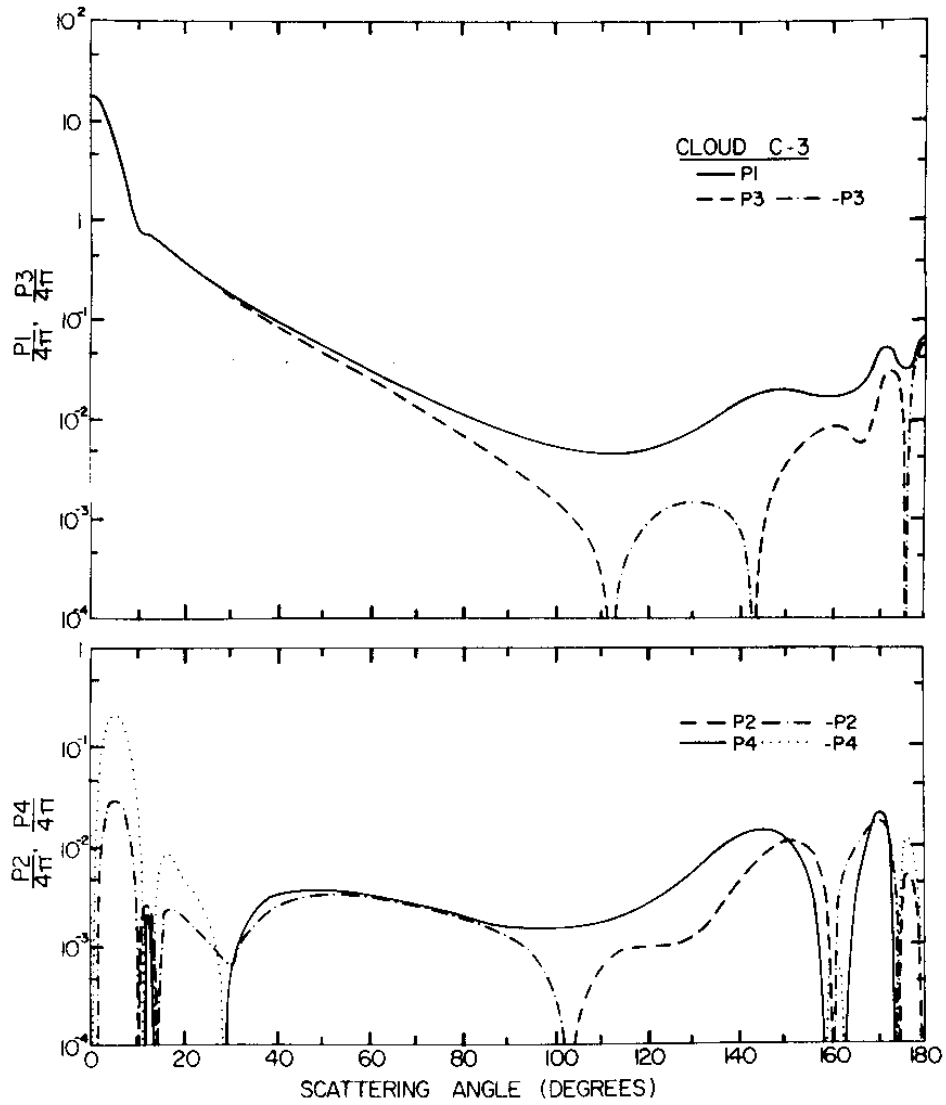about the abscissa.)

Fig. A.5 Scattering matrix elements for cloud model C-3.
(Note that negative terms, indicated in key, are reflected
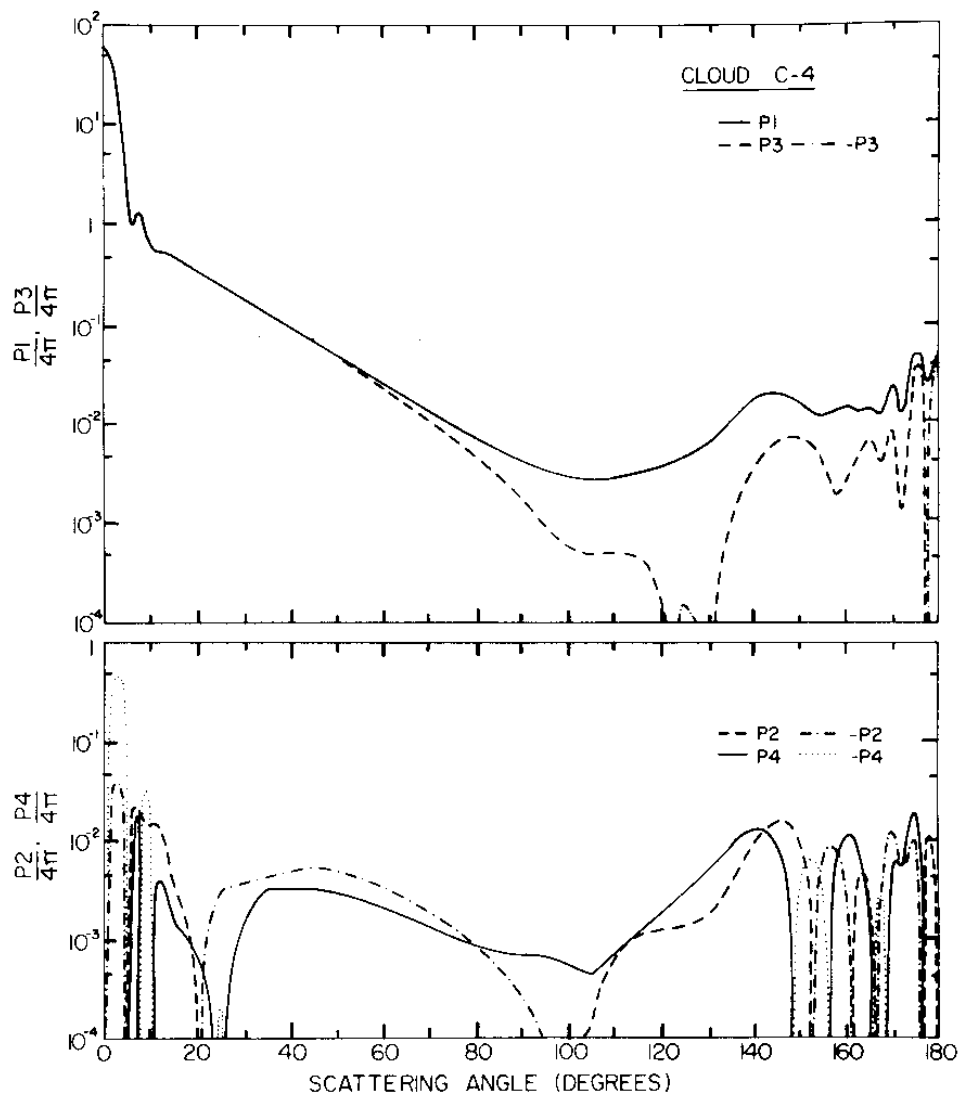about the abscissa.)

Fig. A.6 Scattering matrix elements for cloud model C-4.
(Note that negative terms, indicated in key, are reflected
about the abscissa.)

forward scattering. This enhancement is produced by dif-
fraction effects and is commonly referred to as the dif-
fraction peak. It is useful to examine this feature of the
scattering matrix carefully because the multiply scattered
lidar return is strongly dependent on both its intensity
and angular width.

Weinman (1968) has suggested that the diffraction peak
might be approximated with a Gaussian function of the scat-
tering angle. Because the forward scattering peak is pri-
marily a diffraction effect, Babinet's principle* can be
used to guess that approximately one-half of the energy
scattered by the droplets is contained under this peak.
This fact suggests a way to select a Gaussian approximation
to the diffraction peak: first the amplitude is chosen such
that it is equal to the value of $P_1(\theta)$ at zero scattering
angle.

$$P_1(\theta) = P_1(0) \cdot e^{-\theta^2/\langle\theta^2\rangle} \qquad A.6$$

then $\langle\theta^2\rangle$ is selected from the requirement that half the
energy be under the diffraction peak as follows

---

*Babinet's principle states that the diffraction pattern
due to an opaque screen is the same for the screen and its
compliment. In the complimentary screen all of the origi-
nally opaque areas are transparent, and all the originally
transparent areas are opaque. See Jackson (1962) for more
discussion of this principle.

$$\frac{1}{2} = \frac{P_1(0)}{4\pi} \int_0^{2\pi} d\phi \int_0^{\infty} e^{-\theta^2/\langle\theta^2\rangle} \cdot \theta \cdot d\theta \qquad \text{A.7}$$

solving for $\langle\theta^2\rangle$ yields

$$\langle\theta^2\rangle = \left(\frac{1}{2\pi}\right) \cdot \left(\frac{4\pi}{P_1(0)}\right) \qquad \text{A.8}$$

Because at small scattering angles, diffraction by a circular disk is proportional to the Bessel function expression $\left|\frac{J_1(\text{constant} \cdot \theta)}{\theta}\right|^2$, it can easily be shown that $\frac{d P_1(\theta)}{d\theta} = 0$ at $\theta = 0$. Therefore the above Gaussian yields both the exact magnitude and slope of the matrix element $P_1(\theta)$ at $\theta = 0$. In Fig. A.7 the above Gaussian approximation is compared to the diffraction peaks derived by Deirmendjian from Mie theory.
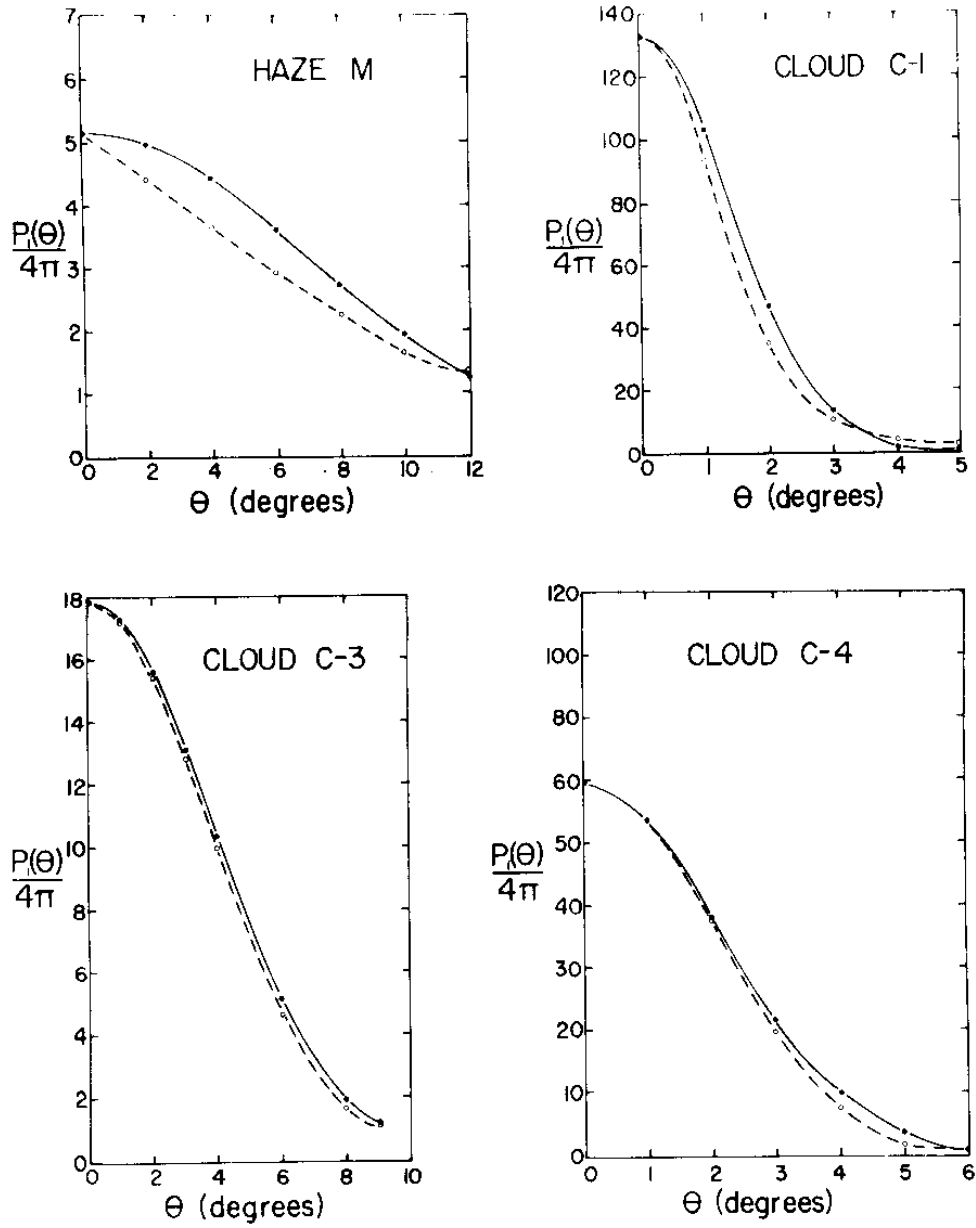
Fig. A.7 A comparison of $P_1(\theta)/4\pi$ (solid lines) for small angle scattering with the gamma function approximation to the diffraction peak (Eq. A.6) (dashed lines). The values of $P_1(\theta)/4\pi$ are the same as those presented in Figs. A.2–A.6.

APPENDIX B   OPERATIONAL DEFINITION OF THE STOKES VECTOR

The Stokes vector components describing a beam of light can be obtained from measurements of the irradiance transmitted through polarizing filters as follows:

$$I = \mathcal{I}_{90°} + \mathcal{I}_{0°}$$
$$Q = \mathcal{I}_{0°} - \mathcal{I}_{90°}$$
$$U = \mathcal{I}_{45°} - \mathcal{I}_{315°}$$
$$V = \mathcal{I}_{RC} - \mathcal{I}_{LC}$$

where: $\mathcal{I}_{\alpha}$ = irradiance transmitted through an ideal linear polarizing filter placed perpendicular to the incident beam with its transmitter axis rotated about the beam by an angle α with respect to an arbitrary reference direction.

$\mathcal{I}_{RC}$ = irradiance transmitted through an ideal right circular polarizing filter.

$\mathcal{I}_{LC}$ = irradiance transmitted through an ideal left circular polarizing filter.

From symmetry argument in the coaxial core
of the lidar problem, with spherical droplets, $U \equiv 0$ and $V \equiv 0$

notice intensity measured, I_m; with a linear polarizing filter

$$I_m = \tfrac{1}{2}(I + Q\cos 2\psi + U\sin 2\psi)$$

since $U \equiv 0$

$$I_m = \tfrac{1}{2}(I + Q\cos 2\psi)$$

REFERENCES

Battan, L.J. and C.H. Reitan (1957) Droplet Size Measurement in Convective Clouds, in _Artificial Stimulation of Rain_, ed. H. Weickmann and W. Smith. London: Pergamin Press.

Chandrasekhar, S. (1960) _Radiative Transfer_. New York: Dover.

Collis, R.T.H. (1969) Lidar. _Advances in Geophysics_. New York: Academic Press.

Curran, R.J. (1971) A Numerical Solution to the Horizontally Inhomogeneous Time-Dependent Transfer Equation. University of Arizona, Ph.D. thesis.

Deirmendjian, D. (1964) Scattering and Polarization Properties of Water Clouds and Hazes in the Visible and Infrared. _Appl. Opt._, 3, 187.

Deirmendjian, D. (1969) _Electromagnetic Scattering on Spherical Polydispersions_. New York: Elsevier.

Diem, M. (1948) Messungen der Grosse von Wolkenelementen II. _Rundschau_, 1, 261.

Jackson, J.D. (1962) _Classical Electrodynamics_. New York: John Wiley and Sons, Inc.

Kattawar, G.W. and G.N. Plass (1968) Radiance and Polarization of Multiple Scattered Light from Haze and Clouds. _Appl. Opt._, 7, 1519.

Kerker, M. (1969) _The Scattering of Light and Other Electromagnetic Radiation_. New York: Academic Press.

Liou, K. (1970) Calculations of Multiple Backscattered Radiation and Depolarization from Water Clouds for a Collimated Pulsed Lidar System. New York University: Geophysical Sciences Laboratory Report TR-70-8.

Liou, K. (1971) Time Dependent Multiple Backscattering. J. Atmos. Sci., 28, 824.

Liou, K. and R.M. Schotland (1971) Multiple Backscattering and Depolarization from Water Clouds for a Pulsed Laser. J. Atmos. Sci., 28, 772.

Perrin, F. (1942) J. Chem. Phys., 10, 415.

Plass, G.N. and G.W. Kattawar (1971) Reflection of Light Pulses from Clouds. Appl. Opt., 10, 2304.

Priebe, J.R. (1969) Operational Form of the Mueller Matrices. J. Opt. Soc. Am., 59, 176.

Rossi, B. (1952) High-Energy Particles. Englewood Cliffs, N.J.: Prentice Hall, Inc.

Schotland, R.M., E. Chang and J. Bradley (1965) Optical Sounding II. Fort Monmouth, N.J.: U.S. Army Electronics Command.

Schotland, R.M. and N.M. Reiss (1970) Double Scattering Computations for a Bistatic Laser Radar System Operating in the Normal (long pulse) Mode. J. Geophys. Res., 75, 7581.

Shurcliff, W.A. (1962) Polarized Light. Cambridge, Mass.: Harvard University Press.

van de Hulst, H.C. (1957) Light Scattering by Small Particles. New York: Wiley and Sons, Inc.

Weinman, J.A. (1968) Axially Symmetric Transfer of Light
   Through a Cloud of Anisotropically Scattering Particles.
   Icarus, 9, 67.